4/

D1.5
Chevrel phases

Damian P Hampshire

D1.5.1 Introduction

Chevrel phase superconductors are a class of materials that have generated enormous interest in the superconductivity community. There are more than 100 different Chevrel phase compounds that exhibit a wide range of properties of both fundamental and technological interest. They have the chemical formula $M_xMo_6X_8$ where x can range from 1 to 4, M can be one of more than 25 different elements and X is usually one of the chalcogenides (S, Se or Te). The structure can incorporate elements of different size, concentration and oxidation state. Some of the most intensively studied Chevrel phase materials with superconducting critical temperatures above 2 K are listed in table D1.5.1 [1–5]. Figure D1.5.1 shows the critical temperature,magnetic ordering temperature and some structural properties of Chevrel phase materials with rare-earth ions [1, 2, 6–8].

Chevrel phase compounds were discovered in 1971 [9]. Interest has been focused on the $PbMo_6S_8$ and $SnMo_6S_8$ materials with high upper critical fields ($B_{c2} \sim 40-60$ T) and T_c values of $\sim 12-15$ K. The B_{c2} values of these Chevrel phase compounds lie between those of the high temperature copper oxide superconductors (e.g. $Bi_2Sr_2Ca_2Cu_3O_x$) and the intermetallic low temperature superconductors (e.g. Nb_3Sn) which means the superconducting coherence length is sufficiently long to reduce the effects of granularity found in high temperature superconductors but sufficiently short for very high field applications. Powder-in-tube wires have been fabricated (cf figure D1.5.2 [10–12] with high critical current densities in high magnetic fields [10, 13, 14] in single lengths up to 1 km long (cf Chapter B3.3.5). This opens the possibility that these materials will be used in the next generation of high field applications operating at magnetic fields significantly above 25 T [12].

In addition to technological interest in these materials, the fundamental interest includes studies of many compounds which include rare-earth elements that are found to exhibit the coexistence of superconductivity and long range magnetic order [15–18] and studies of whether Chevrel phase compounds belong to a new class of (non-BCS [19]) superconductors that include the cuprates and is characterized by relatively high critical temperature for such small n_s/m^* (carrier density/effective mass) [20].

D1.5.2 Structural properties

The majority of superconducting Chevrel phase superconductors are rhombohedral–hexagonal in structure with space group $R\bar{3}$. A schematic presentation of the structure, as well as a simplified cubic structure, is illustrated for $M_xMo_6X_8$, where M is Pb and X is S, in figure D1.5.3 [21]. The sides of all the axes of the rhombohedron are equal and inclined at the same angle ($\sim 90°$) to each other and hence can also be considered a slightly distorted cubic structure. The Pb is almost at the centre of the central cube. At the corners of the central cube are the tightly bonded Mo_6S_8 clusters. Mo forms an octahedron such

Table D.1.5.1. The Critical temperature of Chevrel phase materials and related compounds: the critical temperature (T_c) [1, 2]; the rhombohedral angle, the rhombohedral lattice parameter and the Mo–Mo intracluster spacing [3–5]

Compound	T_c	Rhombohedral lattice parameter (Å)	Rhombohedral angle	Mo–Mo intracluster distance
$PbMo_6S_8$	15 K	6.55	89.4	3.27
$SnMo_6S_8$	13 K	6.52	89.7	3.23
$AgMo_6S_8$	9 K	6.48	92.0	3.15
$ScMo_6S_8$	3.6	–	–	
YMo_6S_8	3.0	6.45	89.5	
VMo_6S_8	8.2	–	–	
$NbMo_6S_8$	3.5	–	–	
$LaMo_6S_8$	7.1	6.51	88.9	
Mo_6S_8	1.6	6.43	91.3	3.08
$Cu_{1.8}Mo_6S_8$	11	6.48	94.9	3.24
$C_{3.2}Mo_6S_8$	6.4	–	–	3.34
$Cu_4Mo_6S_8$	< 1 K	6.59	95.6	3.39
$Cd_{1.1}Mo_6S_8$	3.5	6.52	92.8	
$Li_4Mo_6S_8$	4.4	6.62	94.5	
$Mg_{1.14}Mo_6S_8$	3.5	6.51	93.6	
$Cu_{1.2}Mo_6S_8$	5.6	–	–	
$Zn_{1.1}Mo_6S_8$	3.6	6.49	94.7	
$Cu_2Mo_6S_6O_2$	9	6.54	95.51	
$PbMo_6S_8O_2$	11.7	6.52	88.98	
$PbMo_6Se_8$	6.7	6.81	89.23	
$SnMo_6Se_8$	6.8	6.75	89.4	
$AgMo_6Se_8$	6	6.73	91.7	
$Cu_{2.8}Mo_6Se$	6	6.79	94.9	
Mo_6Se_8	6.4	6.79	94.9	
$Mo_6Se_{4.8}Te_{3.2}$	2.7	–	–	
Mo_6Se_7Br	7.1			
$Mo_6S_6Br_2$	13.8			
$Mo_6S_6I_2$	14.0			
Mo_6Se_7I	7.6			
$Mo_6Te_6I_2$	2.6			
$Mo_4Re_2Te_8$	3.5			
$Mo_6S_{4.8}Te_{3.2}$	2.7			

that each Mo atom is slightly outside the middle of the faces of the S-cube. The Mo_6S_8 is bound together as a cluster with weak intercluster Mo–Mo bonds. The sides of the unit cell are about 6.5 Å and those of the Mo_6S_8 cluster about 3.8 Å. The 4d orbitals of the Mo ions are well extended, so they favour the metallic bond. The clusters are rotated through ~25° about the ⟨111⟩ and thus form the channels in which the M atoms are located. The bond lengths of the Mo_6X_8 cluster in ternary Chevrel phase materials are generally similar to those of the binary parent compounds. All the compounds have metal–metal bonds within the cluster. An important structural feature that affects superconducting properties is the Mo–Mo intracluster distance, which can vary from 3.1 to 3.6 Å (cf table D1.5.1), and which is correlated with the number of valence electrons on the Mo_6S_8 cluster [22]. The iono-covalent

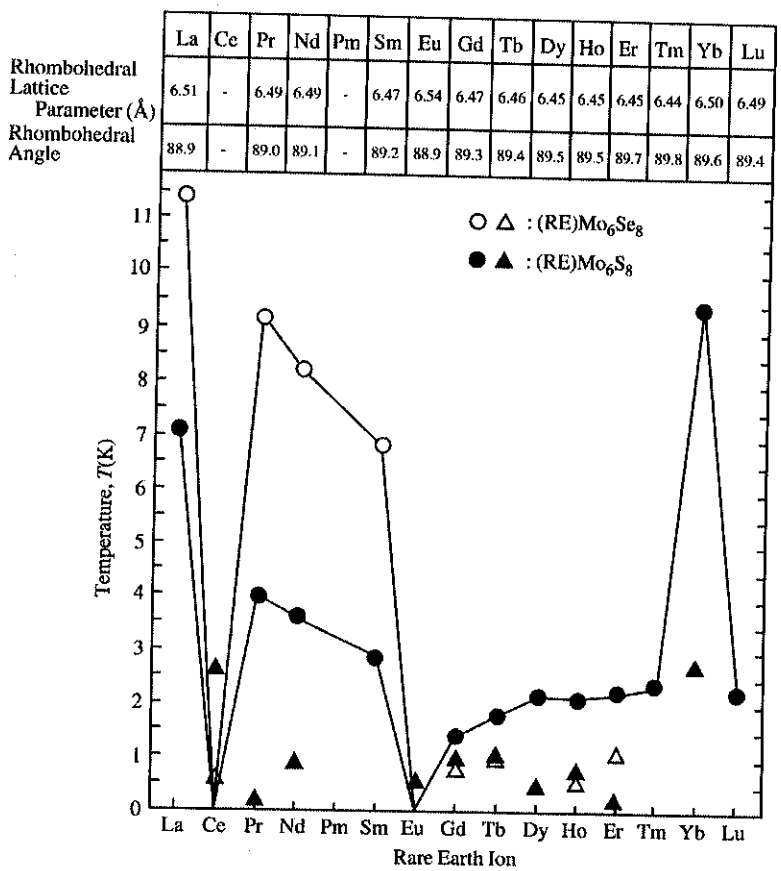

Figure D1.5.1. The rare-earth Chevrel phase superconductors: the critical temperature (T_c: ○ ●), the magnetic ordering temperatures (△ ▲) [1, 2, 6, 7]; the rhombohedral angle and the rhombohedral lattice parameter [5]. No single crystals of heavy rare-earth selenides (i.e. Gd–Yb) have yet been obtained [8] — two phase samples with Mo_6Se_8 ($T_c \sim 6.4$ K) are produced.

cluster–cluster bond can be doped from an insulating state to produce a metallic bond that is superconducting. Chevrel phase compounds can be divided into two types — stoichiometric and non-stoichiometric.

(a) Stoichiometric compounds of $M_xMo_6X_8$ contain large cations such as Pb, Sn, Ag and the rare-earth elements. The structure basically accommodates 1 M ion in one of the six positions which are sufficiently close together to appear as a single site. There is a narrow range of M solubility. All stoichiometric compounds crystallize in the rhombohedral structure at high temperatures with the rhombohedral angle between 88 and 90°. A typical x-ray diffraction pattern for $PbMo_6S_8$ is shown in figure D1.5.4 [23]. The positions of the main diffraction lines and *h*, *k*, *l* indices for the Chevrel phase compound $PbMo_6X_8$ and the most important second phases are given in table D1.5.2.

(b) Non-stoichiometric compounds contain small ions such as Li, Cu and Zn. The rhombohedral angle is between 92 and 95°. The structure can accommodate more than one ion. Figure D1.5.5 shows the possible sites for Cu in the inner cube of the Chevrel phase structure [5]. There are six inner sites and six outer sites. The sites for the small cations depend on the particular cation. With In for example, only

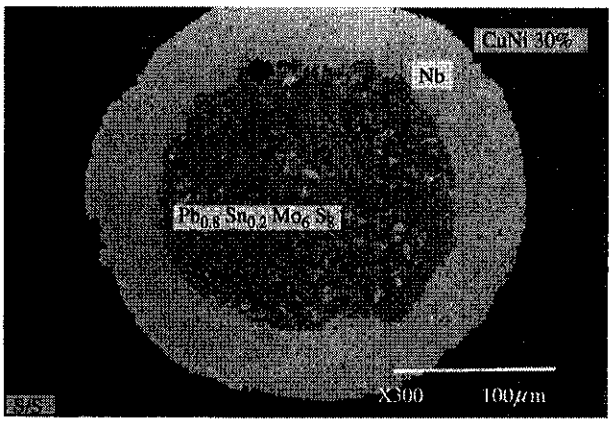

Figure D1.5.2. A $Pb_{0.6}Sn_{0.4}Mo_6S_8$ powder-route wire (from [10] and [11]) which has a critical current density value of 6.7×10^8 A m^{-2} at 14 T and 4.2 K [12]. Nb is a diffusion barrier. CuNi30% is a hard material that reduces damage to Nb during drawing. Stainless-steel (S/S) provides additional mechanical strength and precompresses the Chevrel phase core after cool-down.

the six inner sites are available. At low temperatures the M ion will freeze in one position which breaks the rhombohedral symmetry and can favour a phase transition to a triclinic structure.

The structural transformation from high temperature rhombohedral to triclinic ($P\bar{1}$) between 100 and 140 K [24], has been observed in $PbMo_6S_8$ [25] using neutron scattering. Synchrotron data show a much smaller triclinic distortion, which suggests that sample preparation (possibly oxygen contamination [26]) affects the low temperature transformation [27]. The triclinic phase is the stable low-temperature phase for the non-superconducting divalent (Eu^{2+}, Ba^{2+}, Sr^{2+} and Ca^{2+}) molybdenum sulphide Chevrel phases [28]. Steric and electronic effects (principally charge transfer to the Mo_6S_8 cluster) are important in determining the equilibrium structure [8]. Materials with the highest T_c are those metallic compounds adjacent to a structural instability. They may be in a mixed-phase region consisting of both a superconducting rhombohedral phase and an insulating triclinic phase [28]. The structural instability can result either from changing the cation (chemical pressure) or applying pressure directly [24]. A similar structural instability is found in some of the A15 superconductors which undergo a shear martensitic transformation at some temperature above T_c [29].

The structure of $Cu_xMo_6S_{8-y}$ has been studied in detail below 300 K. Four different low temperature modifications of the rhombohedral phase have been observed [30]. For $x = 1.2$, $T_c = 5.6$ K, for $x = 1.8$, $T_c = 11$ K, for $x = 3.2$, $T_c = 6.4$ K and for $x = 4$ the material is not superconducting [18]. Less detailed studies have also been completed on Ni molybdenum sulfides and selenides.

Solid solutions of Chevrel phase materials can generally be fabricated if the end compounds exist. The solution can either occur with the chalcogenides (e.g. $M_xMo_6Se_{8-x}S_x$) or with the M-elements [17]. Neutron measurements show that in the ternary Pb- and Sn- Chevrel phase sulphides, oxygen can substitute for sulfur which strongly affects the superconducting properties [31]. Of note is the $EuMo_6Se_8$ compound in which either a vacancy or oxygen substitution for Se causes the Eu to move 0.9 Å away from the usual central site [32]. Low level doping of 1–1.5 at% Pb or rare-earth ions into the Chevrel phase binary compound Mo_6Se_8 has also been reported [33, 34].

Detailed TEM has been performed on a range of bulk samples of $(Pb,Gd)Mo_6S_8$ and used to show that material can be produced with coherent tilt grain boundaries. Figure D1.5.6 shows typical data demonstrating that in good material the grain boundaries are free of second phase. In some cases, dislocations are observed that occur at regular intervals along the boundary [11]. Detailed HREM on

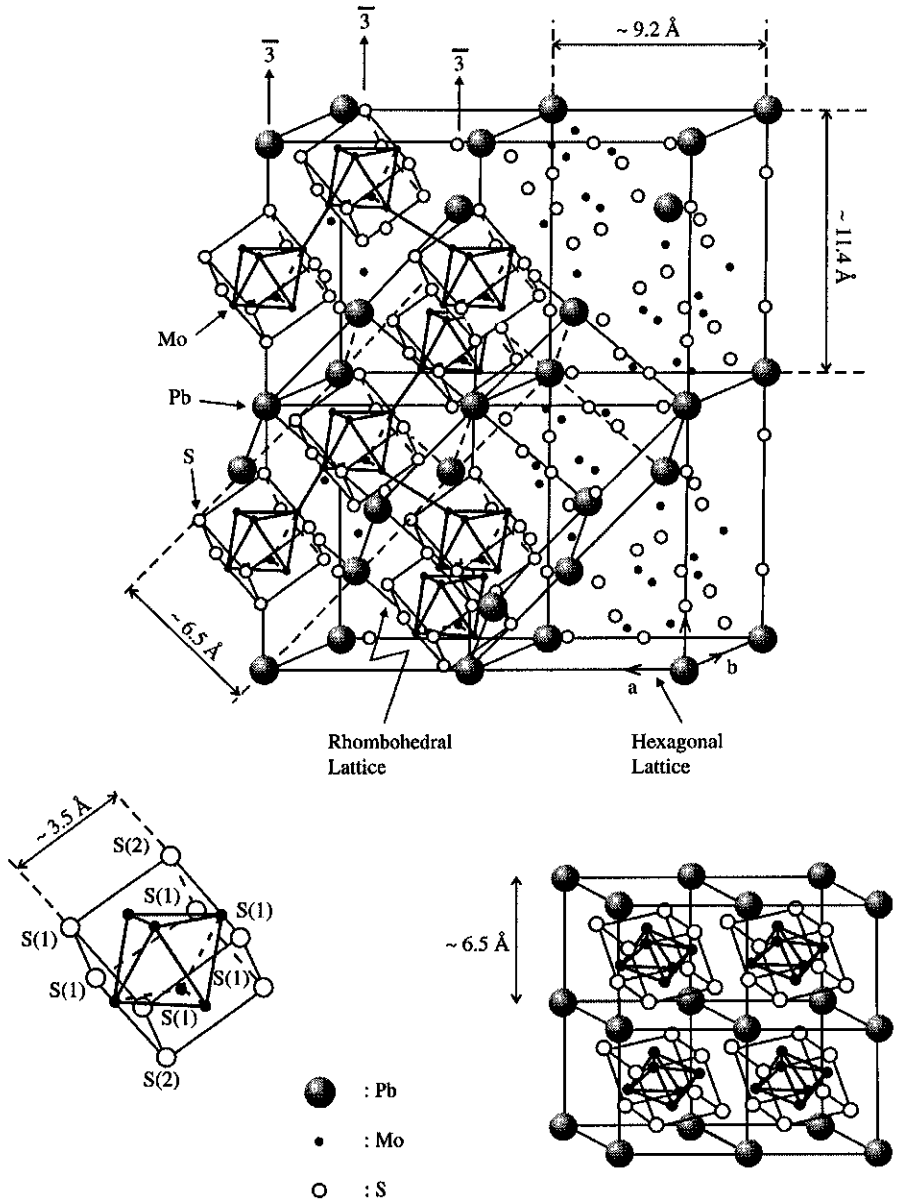

Figure D1.5.3. A schematic of the rhombohedral and cubic structure of $PbMo_6S_8$ [21].

$Ni_2Mo_6S_8$ has shown that edge dislocations, which include an extra plane of Mo_6S_8 clusters, can form. Both coherent and incoherent interfaces have been found in this Ni-based compound [35]. A small number of sulfur defects in the clusters were observed (i.e. $Ni_2Mo_6S_{7.6}$).

There is limited work on structures that occur at very high pressures and temperatures (30–80 kbar and 1200°C). Preliminary work suggests that a metastable structure can be formed in the $PbMo_6S_8$ system [36] at high pressure which has a T_c enhanced by about 1 K but a severely reduced upper critical field (~7 T).

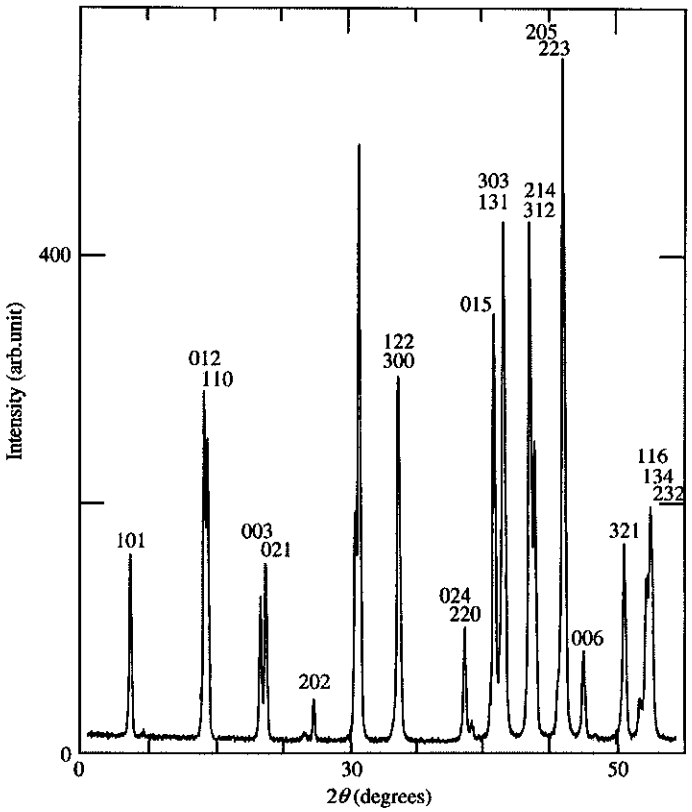

Figure D1.5.4. CuKα powder x-ray diffraction powder pattern for a typical single phase $PbMo_6S_8$ sample [23].

D1.5.3 Thermal properties

The specific heat capacity (C_P) of $PbMo_6S_8$ has been measured by a number of authors in high magnetic fields up to 24 T [37–39]. The electronic contribution in the normal state is $\sim 7\,mJ\,K^{-2}(g\,atom)^{-1}$. In the superconducting state, in addition to the BCS exponential gap term, there is also the term linear in temperature that accounts for the normal cores of the fluxons in the mixed state. At the superconducting jump C/T is $\sim 70\,mJ\,K^{-2}(g\,atom)^{-1}$ which is relatively high because of the soft modes present [40] and $\Delta C_e/T_c$ is about $12\,mJ\,K^{-2}(g\,atom)^{-1}$. The effective Debye temperature measured using C_P measurements changes by a factor of 2 from ~ 200 K at 4.2 K up to ~ 400 K at room temperature [41]. Figure D1.5.7 shows a Debye plot for a series of compounds of the form $Pb_{1-x}Cu_{1.8x}Mo_6S_8$ [23]. Ultrasonic measurements give an average Debye temperature of ~ 245 K [26]. Many magnetic Chevrel phase superconductors have been measured [4]. Such work includes investigating pressure-induced re-entrant superconductivity [42] and the reduction in $\Delta C_e/T_c$ with increased magnetic doping [43]. Nevertheless, there is typically a factor of 2 variation in all the parameters derived from specific heat data in the literature (N.B. for $PbMo_6S_8$, 1 mole = 1037 g = 15 g atom). The differences are attributed to the sensitivity of the materials to the fabrication process.

The consensus on the phonon density of states in Chevrel phase materials is good. The weighted phonon density of states for $PbMo_6S_8$ and $SnMo_6S_8$ measured using neutron scattering measurements and specific heat measurements is consistent with calculations that assume the Mo_6S_8 clusters are tightly bound but only weakly interact with other clusters or the M ion. There is a relatively flat dispersion curve

Table D1.5.2. The x-ray diffraction lines for $PbMo_6S_8$ and the strong intensity lines (> 10%) for the important impurity phases (Mo, MoS_2, Mo_2S_3, Pb, PbS and S). Radiation: CuKα1, $\lambda = 1.54056$ Å (taken from the International centre for Diffraction data)

2-theta	Int.	*h k l*	2-theta	Int.	*h k l*	2-theta	Int.	*h k l*
	$PbMo_6S_8$			MoS_2			Pb	
13.612	50	1 0 1	14.38	100	0 0 2	29.55	100	1 0 0
19.153	100	0 1 2	32.67	22	1 0 0	33.66	80	1 0 1
19.364	80	1 1 0	33.51	12	1 0 1	42.82	75	–
23.303	50	0 0 3	35.87	10	1 0 2	52.23	75	1 1 0
23.700	40	0 2 1	39.53	58	1 0 3	57.95	75	1 0 3
–	–	2 0 2	44.15	11	0 0 6		PbS	
–	–	1 1 3	49.78	29	1 0 5	25.96	84	1 1 1
30.753	100	2 1 1		Mo_2S_3		30.07	100	2 0 0
–	–	1 2 2	10.48	10	0 0 1	43.06	57	2 2 0
33.666	80	3 0 0	16.28	95	1 0 1	50.97	35	3 1 1
38.730	20	0 2 4	21.06	36	0 0 2	53.41	16	2 2 2
–	–	2 2 0	29.61	35	$\bar{2}$0 1		S	
40.971	40	0 1 5	29.73	26	0 1 1	16.59	10	1 2 1
–	–	3 0 3	31.66	46	1 1 0	19.62	17	2 1 2
–	–	1 3 1	31.66	46	0 0 3	22.08	17	2 2 0
–	–	2 1 4	32.33	16	$\bar{1}$ 1 1	23.28	100	2 2 2
43.938	40	3 1 2	32.89	12	$\bar{2}$ 0 2	23.58	23	1 3 2
–	–	2 0 5	34.46	19	1 1 1	24.30	25	1 2 5
–	–	2 2 3	35.09	37	0 1 2	25.37	23	1 3 3
–	–	0 0 6	36.39	11	$\bar{1}$ 1 2	26.05	49	0 2 6
–	–	3 2 1	39.04	28	$\bar{2}$ 0 3	26.84	34	3 1 1
–	–	1 1 6	40.16	58	1 1 2	27.87	36	2 0 6
–	–	1 3 4	40.72	39	2 0 2	28.86	36	1 3 5
–	–	2 3 2	41.03	24	$\bar{2}$ 1 1	31.60	24	0 4 4
	Mo		42.27	21	$\bar{2}$ 0 4	34.27	13	4 0 0
40.51	100	1 1 0	42.93	100	0 1 3	34.37	13	1 3 7
58.60	16	2 0 0	42.93	100	0 0 4	35.06	11	3 3 3
			43.58	51	$\bar{2}$ 1 2	37.17	11	4 0 4
			46.18	23	$\bar{3}$ 0 2	42.84	12	3 1 9

and a strong peak at about 5 meV, associated with the Einstein mode from the M ion. Modes in the energy range up to 18 meV are associated with the soft external modes of the Mo_6S_8 clusters. The hard internal modes are responsible for the energy range from 18 up to 50 meV [40].

D1.5.4 Mechanical properties

Among Chevrel phase materials, the coefficient of thermal expansion (α) has been studied most extensively for $PbMo_6S_8$. Using x-ray diffraction in the range 10–1200 K on bulk material, it has been concluded that α is almost temperature independent up to 900 K (650°C), where $\alpha = 1/L\ (dL/dT) = 9.4 \times 10^{-6}\ K^{-1}$ [44]. For comparison, at room temperature α for $PbMo_6S_8$ is about half that of Cu or steel, about 25% higher than Nb and about twice that of Mo [44]. Single crystal measurements show

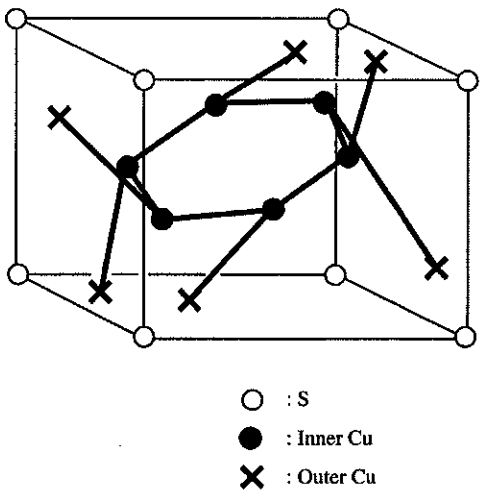

Figure D1.5.5. The possible sites for Cu in the inner cube of $Cu_xMo_6S_8$ [5].

a relatively strong anisotropic variation for α of about a factor 3 [45]. Such considerations are particularly important for optimizing Chevrel phase wires [46]. High resolution thermal expansion measurements have been made using capacitive techniques. These show a very strong change in α at T_c in $PbMo_6S_8$ but not in $SnMo_6S_8$ [47] which was attributed to different coupling between the superconductivity and the orthorhombic–triclinic structural transition (cf chapter B3.3.5).

Compressibilities have been measured for 11 sulfur and selenide Chevrel phase compounds [48] and typical data shown in figure D1.5.8. The Young's's modulus calculated from these data is around 40 GPa [46]. This makes it similar to indium, about a factor of 5 smaller than steel and eight times smaller than Mo. Elastic constants have also been measured using ultrasonic techniques. The elastic constant for transverse distortions is 90 GPa and for longitudinal distortions is 21 GPa [26].

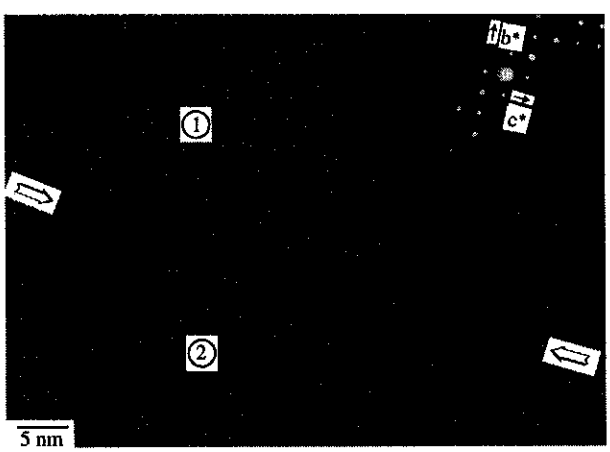

Figure D1.5.6. A high resolution electron micrograph (HREM) of a grain boundary of $Pb_{0.7}Gd_{0.3}Mo_6S_8$ bulk sample. The selected area diffraction pattern (SADP) is for grain (1) and is close to the [100] zone axis. The grain boundary is very narrow [11].

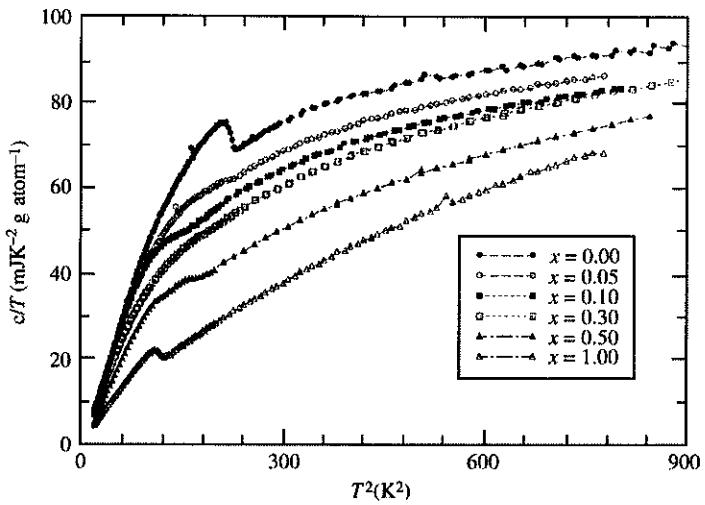

Figure D1.5.7. Debye plot [(heat capacity)^2/(temperature) versus temperature] for $(Pb_{1-x}Cu_{1.8x})Mo_6S_8$ for different values of x [23].

The strain tolerance of Chevrel phase material has been investigated most comprehensively in the context of wires [49]. $PbMo_6S_8$ and $SnMo_6S_8$ fracture at about 0.65%, which is typical for a ceramic material. Mechanical properties such as fracture toughness, crack propagation and fatigue properties are strongly dependent on the porosity of the material. Chevrel phase materials, therefore, can be considered as soft ceramics.

D1.5.5 Chemical properties/phase diagrams

The high vapour pressure of the Pb and S makes accurate phase studies difficult. Very careful exclusion of oxygen and water during material fabrication is required to avoid oxygen substituting for sulfur in the Mo_6S_8 cluster [50] and is necessary for reliable comparisons between structure/composition and superconducting properties. Argon should be used rather than argon–nitrogen since trapped nitrogen can form MoN. Chevrel phase materials start decomposing above 650°C [44]. Most of the important compounds melt in the temperature range from 1500 to 2000°C and the vapour pressure of S or Se (Pb, Sn) is high [7, 51]. Pb, Sn, Ag and rare-earth sulfide and selenide Chevrel phase materials melt peritectically [3]. To make single crystals of the metallic superconductors, a typical off-stoichiometric composition of $Pb_{1.2}Mo_7S_8$ [30] is used and for the rare-earth compounds, $RE_{11}Mo_{38}S_{51}$ [7, 52] and $RE_{15}Mo_{30}Se_{55}$ [8]. These compositions are chosen to produce excess binary chalcogenide which minimizes formation of the Mo_2S_3 phase which competes with the Chevrel phase. Figure D1.5.9 (upper) shows a schematic of the phase diagram for $PbMo_6S_8$ found at ~1000°C [53, 54]. The Mo_2S_3 phase does not form at lower temperatures [55]. The high temperature phase diagram characteristic of the rare-earth compounds is shown in figure D1.5.9 (lower) [7]. The material can be simply cooled from above its melting point to produce single crystals. The final product is generally single crystals in a binary chalcogenide crust which can be separated using HCl diluted with ethyl alcohol (≈ 20 vol% HCl). The natural cleavage planes are the (100) and (110) crystallographic directions [56]. The Cu and Ni sulphide Chevrel phase materials form congruently so that relatively large single crystals can be formed from a stoichiometric melt. In selenium based materials, only single crystals of the light rare-earths have been produced. In heavy

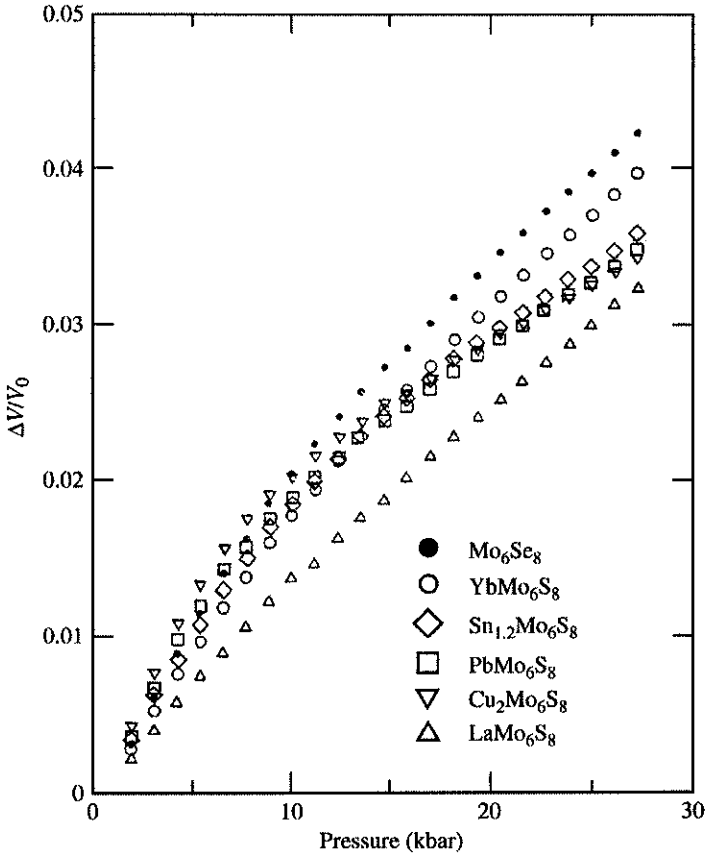

Figure D1.5.8. The compressibility of five ternary molybdenum sulphides $M_xMo_6S_8$ and the binary compound Mo_6Se_8 [48].

rare-earth selenides, RE deficiency produces a two phase sandwich structure of doped binary Mo_6Se_8 and the $REMo_6Se_8$ [8, 57–59].

A number of authors have studied the phase diagrams of the $Pb_xMo_6S_{8-y}$ at 900 [55] and ~1000°C [53, 54]. There is no general agreement about the composition of the Chevrel phase material in the single phase region although many studies show the presence of a small amount of sulfur defects, consistent with HREM studies [35]. Recently it has been concluded [60] that as long as there is no oxygen contamination, the onset of T_c is in the range of 14–15 K, the sulfur stoichiometry is very close to 8 and Pb deficiency is present. Chevrel phase materials have been fabricated at high pressure (typically up to 2000 atm) to increase density and connectivity. It has been suggested that this enhances the effect of oxygen contamination since the material is pushed into a two-phase Chevrel phase + MoS_2 region [47]. Limited work has been completed on decomposition. Since $PbMo_6S_8$ can be formed between 450 and 1650°C, it is reasonable to assume that the structure is very stable. Electron-beam-induced decomposition has been observed in $Ni_2Mo_6S_8$ first showing increased disorder and then, after time, reduction of the Mo_6S_8 clusters giving regions of Mo, Mo–Ni alloy and sulfides [35].

Fine grain, well connected bulk samples are required for high J_c applications. Soft chemistry methods can be used to produce ultrafine precursors (PbS, MoS_2 and Mo) [61]. Alternatively very fine grains of the binary compound Mo_6S_8, which are almost oxygen free, can be formed by leaching the Ni

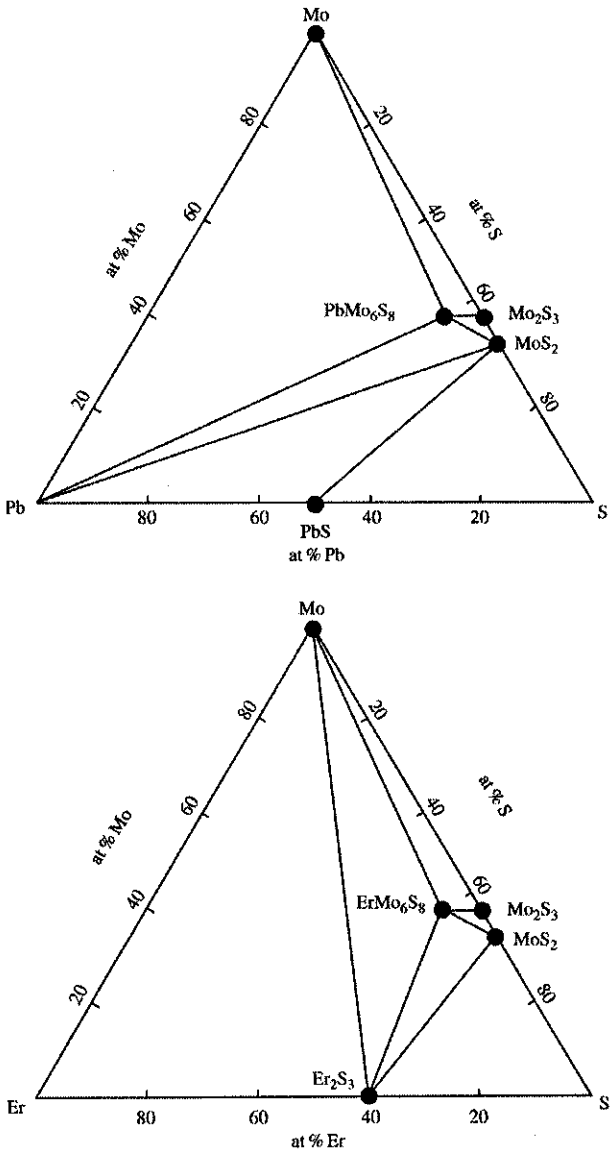

Figure D1.5.9. A schematic of the phase diagram for $PbMo_6S_8$ (upper) [53, 54] and $ErMo_6S_8$ (lower) at temperatures above 1000°C [7].

or Li ions out of the parent Chevrel phase compound using HCl [62, 63]. In this remarkable process, the Ni or Li ions can migrate distances of $\sim 100\ \mu m$ (with potential uses for battery applications). The fine Mo_6S_8 grains can then be used in powder route fabrication of fine grain bulk Chevrel phase materials by reacting with PbS or SnS [64, 65].

Substitutions of Br, I and O for the X element and mixed sulfur–selenium compounds have been fabricated. The Br, I, and O substitutions can increase T_c. Replacing S by Se or vice-versa immediately reduces T_c producing a minimum when there are equal quantities of each element (e.g. $PbMo_6Se_4S_4$).

Most materials in which the Mo element has been substituted (e.g. Nb, Ta, Re, Ru and Rh) are not superconducting [5]. A detailed investigation of the phase diagram at 1200°C in La–Mo–Se has also been completed and the correlation between structural and superconducting properties investigated [57, 66, 67].

D1.5.6 Optical properties

Vibrational Raman spectra have been observed for Cu-, Pb-, Ba- and Sn sulfide Chevrel phase compounds in the range from 10–50 meV [56] as shown in figure D1.5.10. Such measurements give energies and symmetries of the Raman active optical phonons near the Brillouin zero centre. Many peaks are independent of the metal (X) atom even in the non-stoichiometric Cu- compounds, in broad agreement with tunnelling data [68].

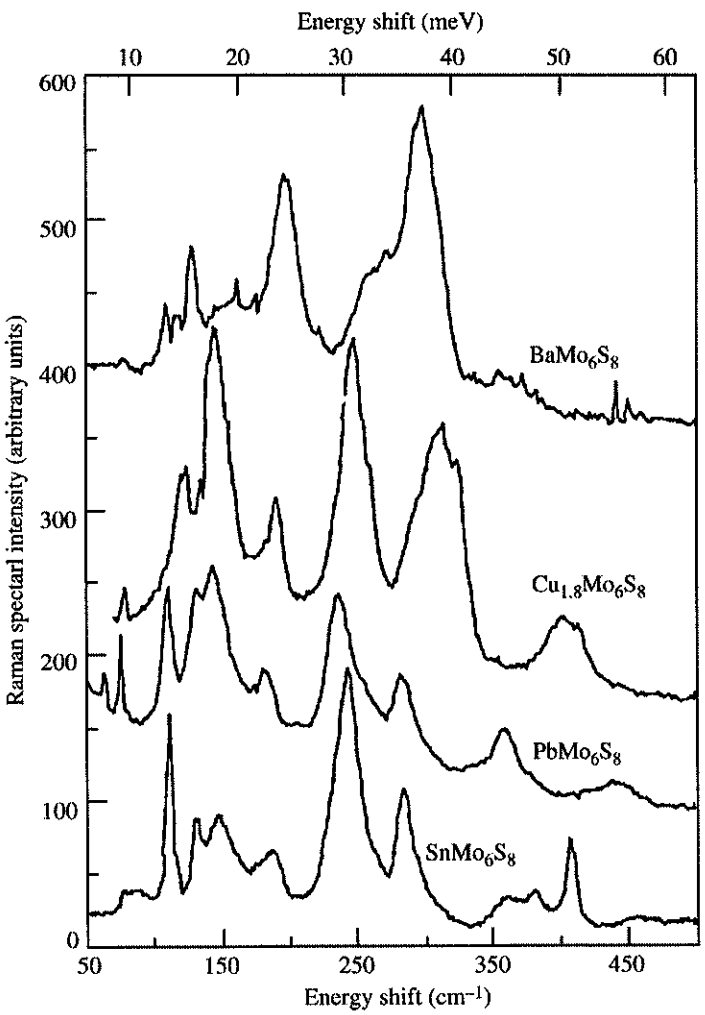

Figure D1.5.10. The Raman spectra for $BaMo_6S_8$, $Cu_{1.8}Mo_6S_8$, $PbMo_6S_8$ and $SnMo_6S_8$ [56].

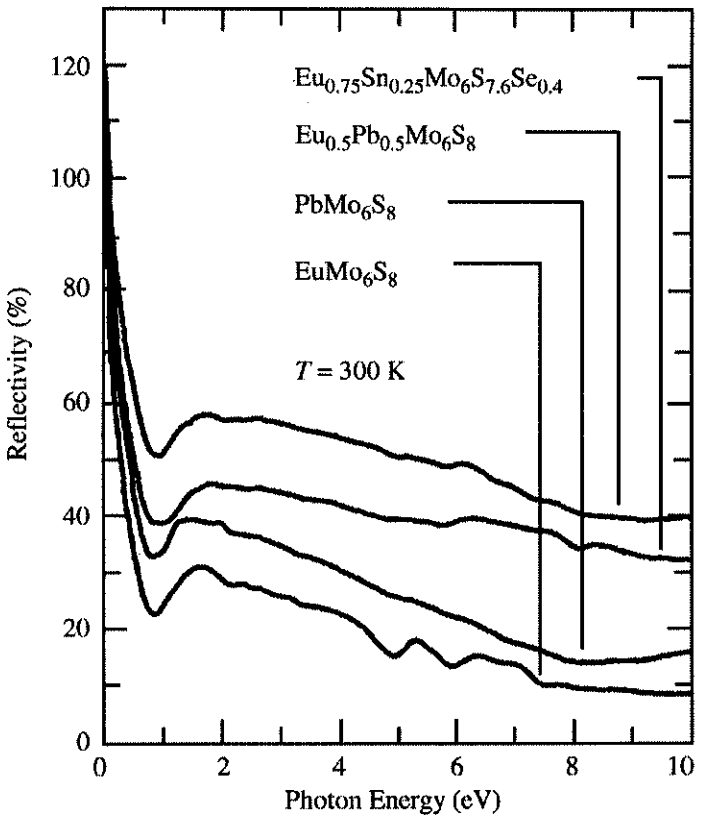

Figure D1.5.11. The near normal reflectivity at room temperature of $EuMo_6S_8$, $PbMo_6S_8$, $Pb_{0.5}Eu_{0.5}Mo_6S_8$ and $Sn_{0.25}Eu_{0.75}Mo_6S_{7.6}Se_{0.4}$ [69].

Reflectivity measurements and complex magneto-optical Kerr-effect measurements have been completed in magnetic fields up to 12 T and temperatures down to 0.5 K [69]. Figure D1.5.11 shows that the reflectivity (and optical conductivity spectra) were similar for $Eu_{1-x}Pb_xMo_6S_8$ and $Eu_{1-x}Sn_xMo_6S_{8-y}Se_y$ at 300 K. The carrier density was low ($\sim 6 \times 10^{27}\,m^{-3}$), the mobility $\sim 1\,cm^2\,V^{-1}\,s^{-1}$ and the effective masses for the carriers $\sim 10\,m_e$.

D1.5.7 Normal state properties

The normal state properties of Chevrel phase compounds are rather well described in terms of their chemistry and are consistent with band structure calculations [70]. The dominant carriers are holes associated with the $4d_{x^2-y^2}$ states. The three important factors that contribute to the electronic properties are the charge transfer from the M cation to the Mo_6S_8 cluster and the volume and structure of the unit cell.

The position of the Fermi level in the sulfide system, is strongly related to the charge transfer between the M cations and the sulfur anions [22]. A characteristic of the Mo_6S_8 cluster is that it is only slightly distorted when filled with 24 electrons and tends to be insulating. The electronic configuration of $Mo4d^5 5s^1$ contributes six electrons to the Mo_6S_8 cluster. Hence with the S in the -2 valence state, there

are 20 electrons in the Mo_6S_8 cluster and there is hole conduction. Adding Pb or Sn to the structure (both have valence +2) increases the number of electrons to 22—equivalent to two holes per cluster which produces the highest value of T_c. For comparison the valence of S, Se and Te in Mo_6S_8, Mo_6Se_8 and Mo_6Te_8 are −2, −1.75 and −1.33, respectively. Band structure calculations show that in the rhombohedral $PbMo_6S_8$, the Fermi energy lies below an energy gap about 1 eV wide [70]. The states near the Fermi energy are strongly confined within the Mo_6S_8 cluster [71]. Indeed there are some broad similarities between Chevrel phase materials and the intercalates of TaS_2 [72] and MoS_2 [73] where there is a hybridization of the metal d-bands and an associated energy gap [74]. The band structures for the Chevrel phase selenides and the telluride have similar properties [71], but one of the marked differences between them and the sulfides is that the density of states at the Fermi energy is higher for trivalent ions than for divalent ions. This is supported by the T_c values which are higher for the rare-earth selenides than for the sulphides as shown in figure D1.5.1.

In $PbMo_6S_8$ samples, the resistivity (ρ) at room temperature is about 100 $\mu\Omega$ cm−1 mΩ cm and typical values for room-temperature-resistivity-ratio (RRR) are 4–6 [23, 44]. In the $Cu_xMo_6S_8$ single crystals, ρ is similar with a RRR value of about 7 which leads to a scattering length (l) of about 20–30 Å [3]. In thin films, RRR values were found in the range 2–6 and l estimated to be ~40 Å [75]. The temperature dependence of $\rho(T)$ is approximately linear up to 50 K but shows negative curvature at higher temperatures similar to the A15 superconductors. Theories that address the non-linearity utilize a strong peak in the density of states [76] or a scattering length that is comparable to the lattice spacing [77]. Experimental data at low temperatures can be misleading, particularly if the material includes pure Mo or Mo_2S_3. Hall effect measurements in the $(Eu_{1-x})Sn_xMo_6S_8$ at room temperature gives Hall coefficients of $+0.7 \times 10^{-3}$ cm^{3}G^{-1} confirming a hole carrier concentration of $\sim 9 \times 10^{27}$m^{-3} [78] (in agreement with the optical measurements and muon measurements [79]) and implying ~2.5 holes per formula unit. In $REMo_6S_8$ compounds, ρ is typically ~300 $\mu\Omega$ cm and RRRs range from 8 to 34 [80], although $LuMo_6S_8$ has a resistivity at room temperature of only 50 $\mu\Omega$ cm [81]. Limited thermopower measurements on $Cu_{1.8}Mo_6S_{8-x}Te_x$ have also been completed [82].

The density of states derived from susceptibility measurements, specific heat measurements and band structure calculations give consistent values. For the Pb- and Sn- Chevrel phase sulfide compounds, χ is about 3.5×10^{-5} emu(g atom)$^{-1}$. The (phonon-enhanced) density of states calculated from C_P measurements is about 1 state per eV-atom-spin. This is about twice that found from χ measurements or bandstructure calculations which is expected with strong electron–phonon coupling [17]. In materials with relatively high critical temperature $PbMo_6S_8$, $LaMo_6S_8$ and $LaMo_6Se_8$, the susceptibility varies by about a factor of 1.5–2 between room temperature and 20 K [7, 67] and shows an anisotropy (for single crystals) of ~40%. A strongly temperature dependent susceptibility has also been observed in high temperature superconductors. This is taken to be evidence that the Fermi level is situated near a peak in the density of states which may cause the relatively high T_c values.

D1.5.8 Superconducting properties

D1.5.8.1 Transition temperature

The theory by Bardeen, Cooper and Schreiffer (BCS theory) [19, 83] currently provides the only generally accepted microscopic explanation for superconductivity. Within this framework, the critical temperature is determined by the density of states at the Fermi level, the phonon spectrum and the electron–phonon coupling. Tunnelling measurements on $Cu_{1.8}Mo_6S_8$ and $PbMo_6S_8$ give the ratio of the gap (Δ) to T_c of $2\Delta/k_BT_c = 4$–5 (BCS theory predicts 3.5) showing strong coupling. In the pseudobinary $Mo_6Se_{1-x}S_x$ system, strong coupling in Mo_6Se_8 ($T_c = 6.2$ K, coupling constant: $\lambda = 1.25$, $2\Delta/k_BT_c = 4.2$, $\Delta C_e/C_e = 2.25$) gives way to weak coupling showing the BCS behaviour in $Mo_6Se_4S_4$ ($T_c = 1.8$ K,

$\lambda = 0.6$, $\Delta C_e/C_e = 1.4$) [84, 85]. Although most of the phonon modes associated with the Mo_6S_8 cluster modes contribute to the electron coupling [86], the higher T_c materials have large values of λ which are probably most strongly affected by the soft modes [84]. The pseudobinary $Mo_6S_6I_2$ compound has the relatively high T_c of 14 K which suggests that the superconductivity in Chevrel phases of highest T_c is fundamentally associated with the clusters. In this context, the isotope effect observed in Mo_6Se_8 is consistent with BCS theory and suggests that an electron–phonon mechanism operates in Chevrel phase materials [85]. For a given structure, T_c also depends on the volume of the unit cell [50] and the valence electron concentration in the Mo_6S_8 cluster. The trivalent sulfur-based Chevrel phase materials have uniformly low T_c whereas the divalent rhombohedral materials have high T_c (e.g. Sn and Pb). Among the trivalent rare-earth ions, there is a correlation between T_c and the volume of the unit cell [17]. When the volume decreases, the inter-cluster Mo–Mo decreases, so the valence bands are expected to broaden, and the density of states and T_c to fall [2]. Hydrostatic pressure has been used to change the volume of the unit cell, and hence T_c, in divalent sulpfides [50, 87, 88]. The effect of pressure on T_c is about an order of magnitude higher than that found in elemental superconductors [89] $dT_c/dP \sim 10^{-4}$ K bar^{-1}. The difference in critical temperature (T_c) between $PbMo_6S_8$ and $SnMo_6S_8$ can be explained by the difference in the volume of the unit cell.

The Chevrel phase materials that transform fully from a rhombohedral structure at high temperatures to a triclinic structure at low temperatures have low electronic density of states [90] and are non-superconducting. However, the superconductivity can be restored if pressure is applied to prevent the triclinic structure occurring. In $BaMo_6S_8$ for example, applying a pressure of 4 GPa changes the material from a triclinic semiconductor to a mixed triclinic–rhombohedral phase that is metallic with a T_c of 12 K [91]. The structural instabilities in the Chevrel phase superconductors may enhance the electron–phonon coupling. In $Eu_{1.2}Mo_6S_8$ [92], (shown in figure D1.5.12) superconductivity close to the metal–insulator transition is tuned by pressure. In $(Sn_{1-x}Eu_xM)_{1.2}Mo_6S_8$ [93] the transition is tuned by Sn content (or carrier concentration). These properties are reminiscent of the HTS materials where high T_c values also occur in materials with relatively low carrier concentration which are in proximity to the metal–insulator transition. There has been intense research into alternative microscopic mechanisms for superconductivity following the discovery of the high temperature superconductors in the late 1980s. There is some empirical evidence that the cuprate and bismuthate high temperature superconductors, the organic, Chevrel-phase and heavy Fermion systems all belong to a single class of superconductors where T_c is proportional to the (small) n_s/m^* (carrier density/effective mass) [20, 94] as shown in figure D1.5.13. In the cuprates, the high values of T_c and the lack of a clear isotope effect suggest a non-phononic mechanism [95]. This suggests that Chevrel phase materials, which have a well-known chemistry and electronic structure, may be model systems in which to investigate non-standard mechanisms for superconductivity because of the simplifications which follow from their (almost) cubic (isotropic) structure. Alternatively, there is evidence that this simple empirical proportionality shown in figure D1.5.13 does not hold in Chevrel phase materials [79] but is best described using a rather more complex percolation model dependence [96]. The microscopic mechanism for superconductivity in the Chevrel phase materials had long been considered classic BCS because of the isotope effect found in Mo_6Se_8, although this is now no longer a closed issue.

D1.5.8.2 Upper critical field

The upper critical field (B_{c2}) is given by

$$B_{c2}(0) \approx \left[8.3 \times 10^{34}\left(\frac{\gamma T_c}{S}\right)^2 + 3.1 \times 10^3 \gamma \rho_N T_c\right] \qquad \text{(D1.5.1)}$$

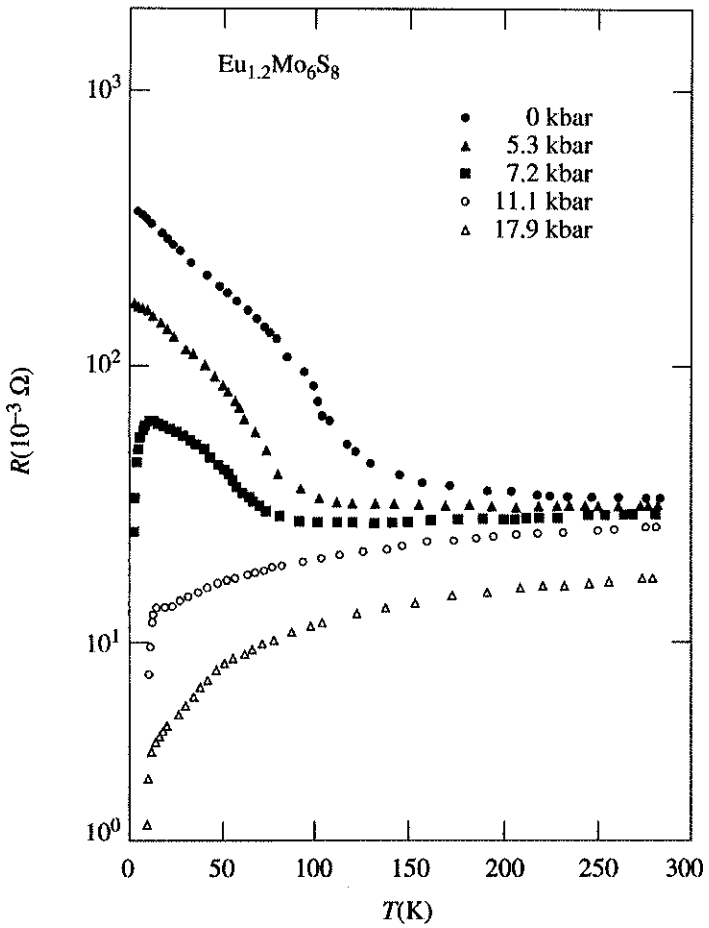

Figure D1.5.12. The resistance versus temperature for $Eu_{1.2}Mo_6S_8$ at various pressures [92].

where the two terms are the clean and dirty contributions, respectively [60, 97], and are consistent with $\xi_0 \sim l$. Both terms contribute to the very high upper critical field values in the $PbMo_6S_8$ and $SnMo_6S_8$ compounds. The effect of the intrinsic spin, orbital coupling and spin-orbit coupling must be included in the Werthamer–Helfand–Hohenberg (WHH) theory to describe the temperature dependence of B_{c2} [98]. However, further theoretical work is still required to assess whether the parameters derived are physically significant. The anisotropy of B_{c2} in $PbMo_6S_8$, $PbMo_6Se_8$ $Cu_{1.8}Mo_6S_8$ and $SnMo_6Se_8$ has been found experimentally to be about 15% [99–101] (as shown in figure D1.5.14) and correlated with the rhombohedral angle (cf Chapter B3.3.5). There is currently no adequate explanation for this since the band structure calculations show nearly cubic symmetry and predict low anisotropy.

D1.5.8.3 Ginzburg–Landau description

Ginzburg–Landau (G–L) theory provides a self-consistent explanation for the properties of metallic superconductors in-field (i.e. superconductors that are non-magnetic in the normal state). There are only two free parameters which can be taken to be the G–L constant (κ) which is temperature independent

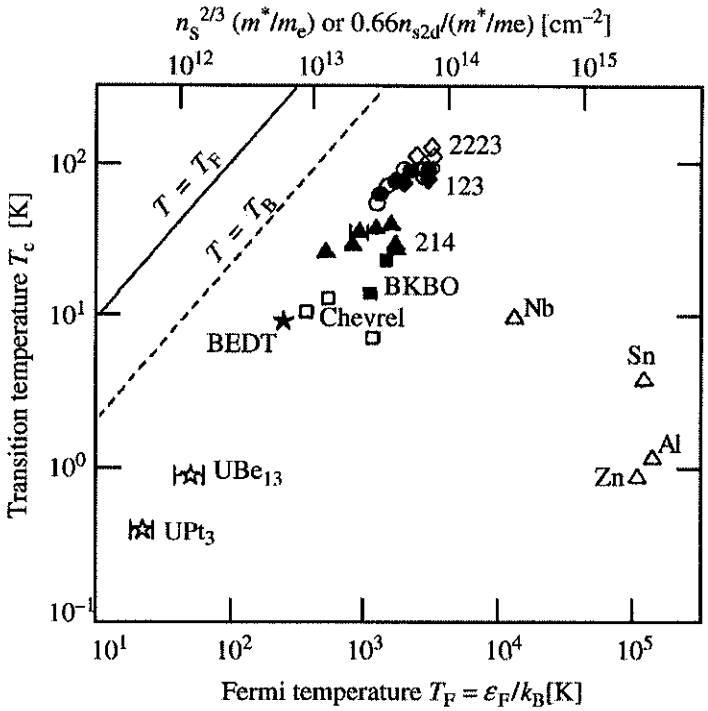

Figure D1.5.13. A log–log plot of critical temperature (T_c) versus the Fermi temperature (T_F) estimated from muon spin resonance measurements (combined with the interplanar distance for two-dimensional and the Sommerfeld constant for three-dimensional systems) for cuprates, BKBO, Chevrel phase, BEDT, heavy-fermion and some elemental superconductors. The dashed line represents the Bose–Einstein condensation temperature, T_B, of the ideal boson gas [20].

and $B_{c2}(T)$ [102]. The fundamental properties of the superconducting state can be determined by measuring the reversible magnetization close to B_{c2} and using the G–L relation:

$$M = \frac{-(H_{c2}-\mathrm{H})}{(2k^2-1)\beta_A} \tag{D1.5.2}$$

where H_{c2} is the critical field strength, H is the applied field strength and β_A is the Abrikosov constant. Reversible magnetization measurements similar to those shown in figure D1.5.15, can be used to obtain values for k and dB_{c2}/dT, from which the slopes dB_c/dT and dB_{c1}/dT can be calculated. For high κ materials such as the Chevrel phase superconductors, it is best not to calculate the critical fields at low temperatures using the G–L relations directly, since G–L theory is strictly only valid close to B_{c2}. In order to calculate $B_{c2}(0)$, the WHH relation can be used where:

$$B_{c2}(0) = -0.7T_c \left.\frac{dB_{c2}}{dT}\right|_{T_c} \tag{D1.5.3}$$

$B_c(0)$ can be calculated using the BCS expression

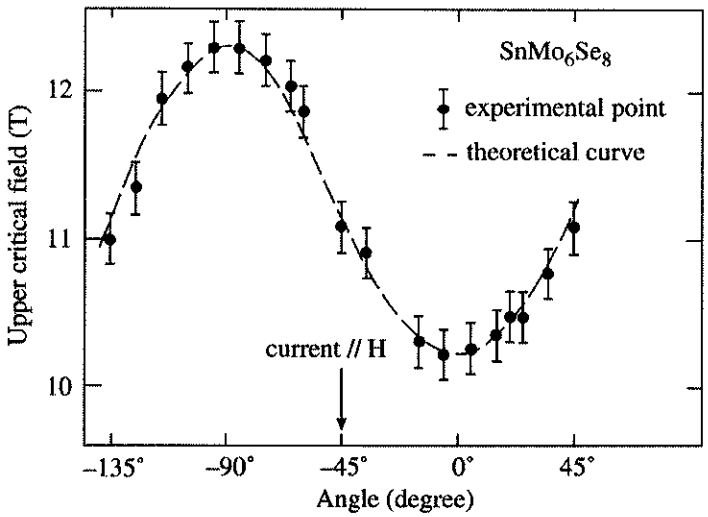

Figure D1.5.14. The anisotropy of the upper critical field of $SnMo_6S_8$ at 4.2 K [99]. The angle is measured between the ternary axis and the magnetic field.

$$B_c(T) = 1.74B_c(0)\left(1-\frac{T}{T_c}\right) \tag{D1.5.4}$$

$B_{c1}(0)$ can be calculated using the Gorter–Casimir [103] two-fluid empirical relation:

$$B_{c1}(T) = B_{c1}(0)\left[1-\left(\frac{T}{T_c}\right)^2\right] \tag{D1.5.5}$$

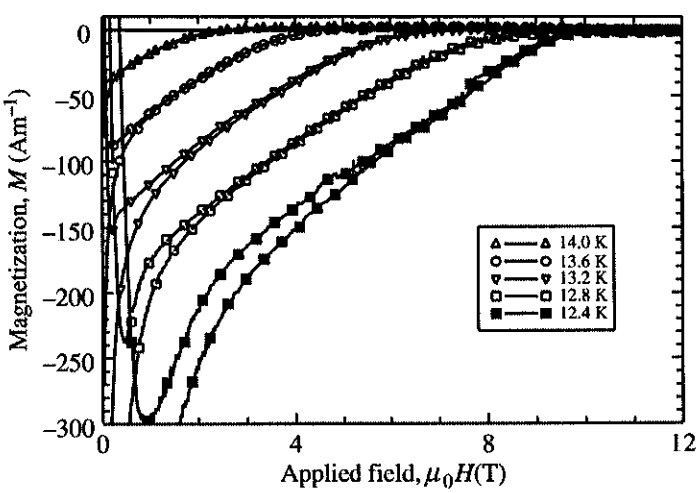

Figure D1.5.15. The magnetization of bulk $PbMo_6S_8$ as a function of field at different temperatures. From the reversible data, one can use G–L theory theory to calculate the G–L parameter and the upper critical field [23, 104].

Table D1.5.3. The values of the fundamental superconducting parameters of $PbMo_6S_8$ derived from reversible magnetization data [104].

T_c	κ	$B_{c2}(0)$	$B_{cl}(0)$	$B_c(0)$	$\lambda(0)$	$\epsilon(0)$
13.7 K	130	56 T	6.4 mT	250 mT	230 nm	2.0 nm

Note that this approach does mean that the G–L relations do not hold at low temperatures [104] — for example, $B_{c2}(0) \neq \phi_0/2\pi\xi^2_{G-L}(0)$. However, more reliable values for the critical fields are found at low temperatures using this procedure. The critical parameters for $PbMo_6S_8$ are shown in table D1.5.3.

The magnetic penetration depth can also be measured using positive-muon spin rotation. This technique allows direct measurement of the variation in the magnetic field throughout the bulk of the sample, from which the penetration depth can be directly measured. The penetration depth has been measured in $SnMo_6S_{8-x}Se_x$ and $PbMo_6S_{8-x}Se_x$ [79]. There is reasonably good agreement between magnetic measurements and muon techniques.

D1.5.8.4 Irreversibility fields

The concept of the irreversibility field (B_{IRR}) is well documented in the literature both in the high temperature and low temperature superconductors [105, 106]. B_{IRR} is the magnetic field (below B_{c2}) at which the critical current density falls to zero. An important experimental problem is that measurements can only determine the field at which J_c drops below a minimum detection level. For practical purposes, a number of techniques are used, although the best procedure to measure B_{IRR} has not been generally agreed.

Vibrating sample magnetometry (VSM) can determine the field which delineates the hysteretic and reversible magnetic properties of a material and hence B_{IRR} directly [102]. Such measurements have been

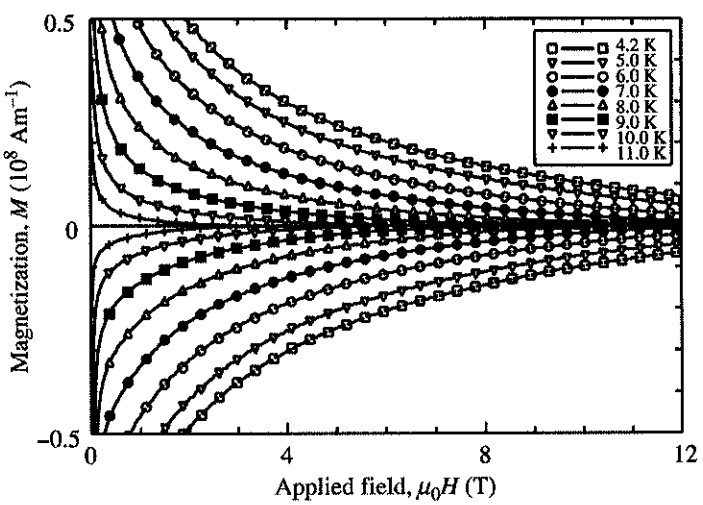

Figure D1.5.16. The magnetization of bulk $PbMo_6S_8$ as a function of field at different temperatures [23]. From the magnitude of the hysteresis, one can calculate the critical current density using Bean's model [109].

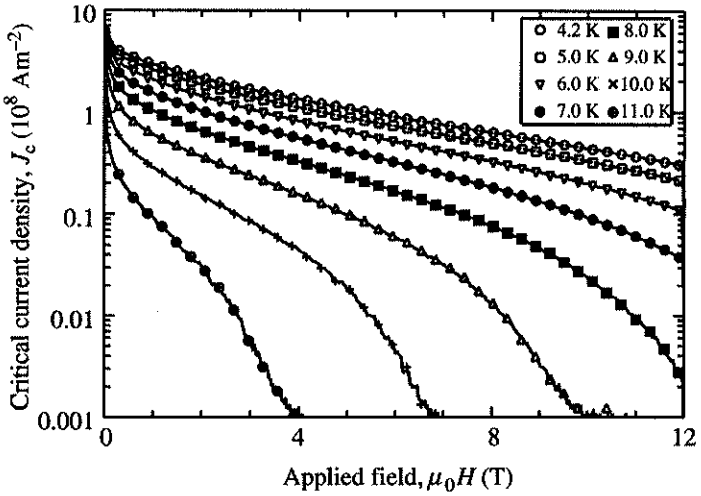

Figure D1.5.17. The critical current density of bulk $PbMo_6S_8$ as a function of field at different temperatures calculated using the data from figure D1.5.14 and Bean's critical state model [23].

performed on $PbMo_6S_8$. In bulk $PbMo_6S_8$, it was found that $B_{IRR} = 63\ (1-T/T_c)^{1.46}$ [104]. A similar power law has been observed in single crystals [105] and derived theoretically using a thermally activated flux-creep model [107]. Measurements have also been completed on $(Pb_{1-x}Gd_x)Mo_6S_8$ that demonstrate that B_{IRR} decreased with increases in Gd content [108]. However, one should be very careful interpreting such data since the hysteresis in magnetization found in VSM measurements can only be simply related to
Q3 J_c using Bean's model [109] if the field applied to the sample is uniform (cf figures D1.5.16 and D1.5.17). However as J_c drops, the hysteresis collapses to zero when the variation in applied field the sample experiences while oscillating is equal to the self field of the sample (although J_c is not zero). For example in figure D1.5.15, although the hysteresis falls dramatically at 12.8 K when the applied field reaches 0.5 T, the anomalous bump (below an extrapolation of the reversible magnetization) is associated with the inhomogenity of the applied field and not related to B_{IRR} at all [110]. In such cases, any comparison of such field values with theoretical calculations of B_{IRR} is compromised, although it is useful to assess practical limits for high field applications.

Flux penetration measurements and transport measurements offer alternative means to measure the critical current densityv [111]. A type of irreversibility field can be determined by extrapolating the functional form of J_c to zero using a Kramer extrapolation [112]. In $PbMo_6S_8$, the irreversibility field has been improved from ~22 T up to nearly 40 T at 4.2 K by fabricating the material using hot isostatic pressing [113]. B_{IRR} values of 35.4 T at 4.2 K have been achieved in high J_c (Pb, Sn) Mo_6S_8 wires [12]. Standard resistance or susceptibility measurements can also be used to determine B_{IRR} [114]. However, values obtained using different techniques can differ markedly. For example, increasing the Gd content in (Pb,Gd) Mo_6S_8 increases the irreversibility field in high-fields measured using the onset of the resistive transition but shows a decrease using the onset of the susceptibility transition [111].

D1.5.8.5 Pinning energies

The apparent pinning energy (U^*) of $PbMo_6S_8$ has been measured using the decay of the magnetization in time [104]. U^* varies from about 40 meV at 2 T to 15 meV at 12 T at 4.2 K. These values are about

double the equivalent values found in $YBa_2Cu_3O_7$ and four times that of $Tl_2Ba_2Ca_2Cu_3O_{10}$ at low fields. Activation energies derived from Arrhenius plots of resistivity give 130 meV at 9 T for $PbMo_6S_8$ and 186 meV at 9 T and 4.2 K for $SnMo_6S_8$ [115]. Comparisons between equivalent measurement techniques suggest that the effect of flux creep is more pronounced in $PbMo_6S_8$ than in NbTi but less than that in high temperature superconductors.

D1.5.8.6 Microwave surface resistance measurements

Very few microwave measurements have been completed on Chevrel phase superconductors. For a superconducting $Cu_2Mo_6S_8$ thin film, a surface resistance of 4.5 mΩ at 10 Ghz and 4.2 K has recently been obtained [116].

D1.5.8.7 Critical current versus field and temperature

The mechanism that determines the critical current density has long been a topic of theoretical and experimental research. J_c is determined both by the intrinsic fundamental superconducting properties and by the extrinsic metallurgical and microstructural factors such as the grain size of the material. Fietz and Webb [117] suggested parameterising J_c through a scaling law for the volume pinning force ($F_P = J_c \times B$). The Chevrel phase materials can be described using this law where

$$F_P = J_c \times B = \alpha[B^*_{c2}(T)]^n b(1-b)^2 \qquad \text{(D1.5.6)}$$

where $B_{c2}{}^*(T)$ is the effective upper critical field, α and n are constants and b is the reduced field $[B/B^*_{c2}(T)]$. The index n is typically between 2 and 3.

In low fields, the parameter α increases as the grain size decreases as is also found in low temperature superconductors such as Nb_3Sn [118]. There are many different approaches to modelling the pinning including that of Kramer after whom the reduced field dependence is named but which is probably not correct in detail [112, 119]. Other pinning models have also been suggested that give the Kramer dependence and emphasize the importance of the grain boundaries. As yet, however, there is no consensus on the nature of the pinning that causes the ubiquitous Kramer dependence [120–122].

In materials optimized for high J_c in high fields, there is a much weaker correlation between J_c and grain size. For example, at 4.2 K in $SnMo_6S_8$, J_c is almost independent of grain size at fields above 15 T [123]. In $PbMo_6S_8$, J_c at 6 T saturates for grain sizes below 0.3 μm [124], although it must be noted that these samples are not fully dense. Kramer found a similar saturation (or peak effect) close to B_{c2} in many low temperature superconductors [125, 126]. The value of field at which J_c extrapolates to zero $[B^*_{c2}(T)]$ is strongly correlated with the properties of the grain boundaries rather than either intragranular properties or the thermodynamic upper critical field [127]. Moreover in contrast to A15 commercial wires [121], during dissipation (above J_c) flux flow is localized along narrow channels [128]. Hence for high J_c materials, the standard grain boundary description may not be appropriate in the high field (or saturation) regime. Whether this is because the efficiency of the grain boundaries falls or because a different (pinning [122, 129] or non-pinning [130]) mechanism limits J_c, remains unresolved.

The influence of neutron irradiation on J_c of Chevrel phase compounds has been investigated and some limited improvements were found [131]. The highest J_c in wires is found in the quaternary $(Pb,Sn)Mo_6S_8$ for which at 4.2 K and 14 T, J_c is 7×10^8 A m^{-2} [10, 12] and at 20 T about 2×10^8 A m^{-2} [132]. Although the Pb based Chevrel phase material has the highest critical field, some Sn is often included in bulk materials. This addition improves the homogeneity of the bulk [133] and the interconnectivity between the grains probably by suppressing formation of MoS_2 [63]. Further improvements in the grain boundaries are still required to increase J_c. Multifilamentary wires have been produced [134, 135], as have monocore wires with Ag [136] Ta [137] and Mo sheathing [14, 138] (cf

Chapter B3.3.5). Small three layer coils have been fabricated using $PbMo_6S_8$ to demonstrate their potential use in magnet applications [139].

A maximum value of J_c for $PbMo_6S_8$ has been estimated at $10^{10}\,A\,m^{-2}$ at 4.2 K and 20 T using a model which assumes ideal arrangement of the pinning sites [105]. Flux penetration measurements with small ac fields have found that $J_c > 10^{10}\,A\,m^{-2}$ at 4.2 K and 5 T at the surface of bulk $PbMo_6S_8$ which demonstrates the potential of this material [140]. Very significant improvements in J_c have been achieved in the high temperature superconductors by fabricating textured material [141]. It remains an open question whether texturing would be useful for increasing J_c in Chevrel phase superconductors.

D1.5.9 The magnetic Chevrel phase superconductors

Very small amounts of magnetic impurities at the parts-per-million level or paramagnetic ions at the 1 at % level are known to destroy the superconducting properties of most superconductors. Ginzburg pointed out that among the elements of the periodic table, superconductivity and magnetism seem to be mutually exclusive [142]. Early experimental work investigating superconductors with magnetic impurities was compromised by uncertainty over whether or not the superconductivity and the ferromagnetism coexisted in the same region of the sample. In Chevrel phase rare-earth materials, however, superconductivity and magnetism coexist within the same unit cell.

The structure of magnetic Chevrel phase superconductors with the rare-earth element centrally located in the unit cell gives a relatively large distance, and hence weak overlap, between the 4d-electrons of the Mo and the 4f-electrons of the rare-earth element. In contrast, the 3d-elements are located close to the Mo_6S_8 cluster and the superconductivity is destroyed. At present there are no single crystals of heavy rare-earth Chevrel phase selenides available (cf section D1.5.5).

Susceptibility measurements show that the ternary magnetic superconductors have an effective Bohr magneton number that is close to the theoretical values for isolated ions at temperature above about 50 K [143, 144]. At lower temperatures, deviations from the Curie–Weiss law occur because of crystal field and magnetic correlation effects. There are many similarities in the superconducting and magnetic properties of the rare-earth Chevrel phase materials and the strongly magnetic nickel–boron-carbide materials [145] and the Rare-earth-rhodium-borides. The properties of $GdMo_6S_8$ are shown in figure D1.5.18 [4, 6]. The re-entrant resistance is correlated with the antiferromagnetic ordering which occurs at 0.82 K as shown by the heat capacity measurements and neutron scattering measurements [4, 146, 147]. The nature of the magnetic ordering is dependent on the particular rare-earth element in the compound and can be antiferromagnetic, ferromagnetic or oscillatory. For example in $HoMo_6S_8$, tunnelling spectrometry suggests that superconductivity coexists with ferromagnetism [148]. In high fields, so called re-entrant superconductivity can occur in some systems [149]. It has been suggested that in high fields, the applied external field compensates for the negative exchange interaction between the rare-earth ion and the conduction electrons so that the material becomes superconducting [150] in a limited part of B–T phase space. The degree to which ordering of the ions is exchange driven [151] and driven by dipolar interactions [149] is still open to discussion.

The range of phenomena of the rare-earth Chevrel phase superconductors continues to fascinate the scientific community. The complexity arises because in order to understand the properties of these materials we must understand how magnetism and superconductivity operate at the atomic level.

D1.5.10 Concluding comments

Since their discovery in 1971, Chevrel phase materials have been of interest to the whole superconductivity community from engineers, who want to make high field magnets, to physicists, who want

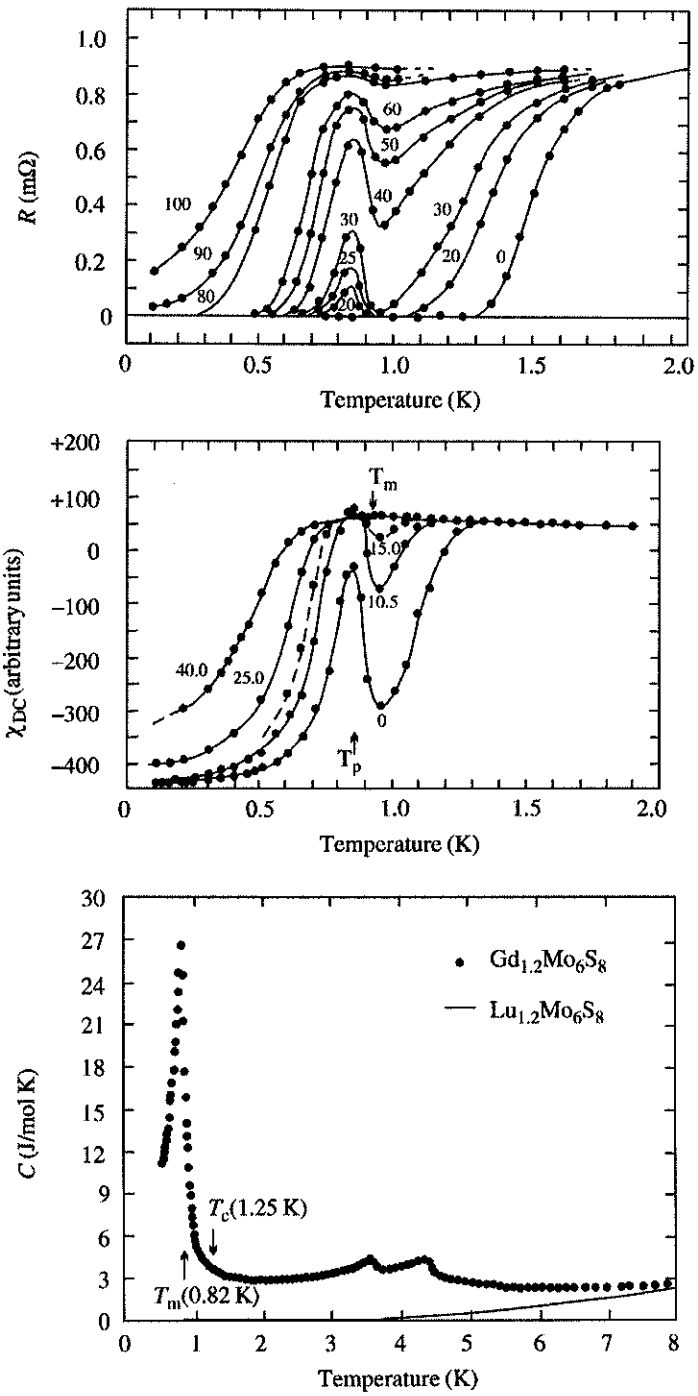

Figure D1.5.18. Selected properties of the magnetic rare-earth compound $GdMo_6S_8$ [6].

to understand the microscopic mechanism that causes superconductivity, magnetism and coexistence of the two. Interest in these materials inevitably waned with the discovery of the high temperature superconductors in 1986 by Bednorz and Muller. Massive interest in HTS materials was driven by the possibility of discovering a new mechanism producing superconductivity and the potential for new applications operating at liquid nitrogen temperatures. Related driving forces are now increasing the research activity into Chevrel phase superconductors. Fundamental interest arises because these materials may offer a model (almost) cubic system in which to address non-BCS superconductivity without the strong anisotropy or layering present in the HTS materials. Furthermore, Chevrel phase superconductors have interesting fundamental properties that are intermediate between the HTS and LTS materials. Technological interest arises because of the high values of B_{c2} in these materials and recent improvements in cryocooler technology which facilitates operating very high field magnets at ~4 K [152]. Indeed if J_c in the wires of these materials can be improved by a factor of ~4, we can expect to use them in the next generation of high field magnet systems operating in fields significantly above 25 T.

Acknowledgments

The author acknowledges helpful comments and literature from the groups in Durham, Geneva and Rennes. He also thanks Amanda, Emily, Peter, Alex and Michael for their support.

References

[1] Shelton R N, McCallum R W and Adrian H 1976 Superconductivity in rare earth molybdenum selenides *Phys. Lett.* **56A** 213
[2] Fischer O, Treyvaud A, Chevrel R and Sergent M 1975 Superconductivity in the $RE_xMo_6S_8$ *Solid State Commun.* **17** 721
[3] Maple M B and Fischer O 1982 *Superconductivity in Ternary Compounds vol I: Structural, Electronic and Lattice Properties* 1st edn (Berlin: Springer)
[4] Maple M B and Fischer O 1982 *Superconductivity in Ternary Compounds vol II: Superconductivity and Magnetism* (Berlin: Springer)
[5] Chevrel R and Sergent M 1982 *Chemistry and Structure of Ternary Molybdenum Chalcogenides*, ed O Fischer and M B Maple p 25
[6] Ishikawa M, Fischer O and Muller J 1982 *Superconductivity and Magnetism in (RE)Mo_6S_8 Type Compounds*, ed O Fischer and M B Maple p 143
[7] Pena O and Sergent M 1989 Rare earth based chevrel phases $REMo_6X_8$: crystal growth, physical and superconducting properties *Prog. Solid State Chem.* **19** 165
[8] Pena O, Geantet C, Schmitt H, Le Berre F, et al. 1999 Structural properties of rare-earth molybdenum chalcogenides $REMo_6X_8$ *Solid State Sci.* submitted
[9] Chevrel R, Sergent M and Prigent J 1971 Sur de Nouvelles Phases Sulfurees Ternaires du Molybdene *J. Solid State Chem.* **3** 515
[10] Cheggour N, Decroux M, Gupta A, Fischer O, et al. 1997 Enhancement of the critical current density in Chevrel phase superconducting wires *J. Appl. Phys.* **81** 6277
[11] Eastell C 1998 Microstructure and properties of high temperature superconducting wires Thesis Oxford University
[12] Cheggour N, Decroux M, Fischer O and Hampshire D P 1998 Irreversible line and granularity in chevrel phase superconducting wires *J. Appl. Phys.* **84** 2181
[13] Yamasaki H, Umeda M and Kosaka S 1992 High critical current densities reproducibly observed for hot-isostatic-pressed $PbMo_6S_8$ wires with Mo barriers *J. Appl. Phys.* **72** 1
[14] Seeber B, Erbuke L, Schroeter V, Perenboom J A A J, et al. 1995 Critical current limiting factors of hot isostatically pressed (HIP ed) $PbMo_6S8$ wires *IEEE Trans. Appl. Supercond.* **5** 1205
[15] Foner S, McNiff E J, Jr and Alexander E J 1974 600 kG superconductors *Phys. Lett.* **49A** 269
[16] Matthias B T, Marezio M, Corenwitt E, Cooper A S, et al. 1972 High temperature superconductors, the first ternary system *Science* **175** 1465
[17] Fischer O 1978 Chevrel phases: superconducting and normal state properties *Appl. Phys.* **16** 1
[18] Niu H J, Morley N A and Hampshire D P 2001 Chevrel phase $(Pb_{1-x}Cu_{1.8x})Mo_6S_8$ with a mixed structure and high critical parameters *IEEE Trans. Appl. Supercond.* **11** 3619
[19] Bardeen J, Cooper L N and Schreiffer J R 1957 Theory of superconductivity *Phys. Rev.* **108(5)** 1175

[20] Uemura Y J, Le L P, Luke G M, Sterlieb B J, et al. 1991 Basic similarities among cuprate, bismuthate, organic, chevrel-phase, and heavy-fermion superconductors shown by penetration-depth measurements *Phys. Rev. Lett.* **66** 2665
[21] Uchida T and Wakihara M 1991 Thermal behaviour of the Chevrel phase sulphides *Thermochim. Acta* **174** 210
[22] Yvon Y and Paoli A 1977 Charge transfer and valence electron concentration in Chevrel phases *Solid State Commun.* **24** 41
[23] Niu H J, Leigh N R and Hampshire D P structure and superconducting properties of $Pb_{1-x}Cu_{1.8x}Mo_6S_8$ *Phys. Rev. B* submitted
[24] Jorgensen J D, Hinks D G and Felcher G P 1987 Lattice instability and superconductivity in the Pb, Sn and Ba Chevrel phases *Phys. Rev.* B **35** 5365
[25] Jorgensen J and Hinks D G 1985 Low temperature structural distortions in the high Tc Chevrel-phase superconductors $PbMo_6S_8$ and $SnMo_6S_8$ *Solid. State Commun.* **53** 289
[26] Wolf B, Molter J, Bruls G, Luthi B, et al. 1996 Elastic properties of superconducting Chevrel-phase compounds *Phys. Rev.* B **54** 348
[27] Francois M, Yvon K, Cattani D, Decroux M, et al. 1994 Synchrotron powder diffraction study of the low-temperature lattice distortion of $PbMo_6S_8$ *J. Appl. Phys.* **75** 423
[28] Jorgensen J D and Hinks D G 1986 Rhombohedral-to-Triclinic phase transition in $BaMo_6S_8$ *Physica* B **136** 485
[29] Batterman B W and Barrett C S 1964 Crystal Structure of Superconducting V_3Si *Phys. Rev. Lett.* **13** 390
[30] Flukiger R and Baillif R 1982 Metallurgy and Structural Transformations in Ternary Molybdenum Chalcogenides, ed O Fischer and M B Maple p 113
[31] Hinks D G, Jorgensen J D and Li H C 1983 Structure of the oxygen point defect in $SnMo_6S_8$ *Phys. Rev. Lett.* **51** 1911
[32] Le Berre F, Pena O, Perrin C, Padiou J, et al. 1998 Novel crystal structure in the Chevrel-phase compound $EuMo_6Se_8$. Transport and magnetic properties *J. Alloys Compd.* **280** 85
[33] Le Berre F, Pena O, Hamard C, Corrignan A, et al. 1997 New superconducting materials based upon doping of the Chevrel phase binary compound Mo_6Se_8 *J. Alloys Compd.* **262** 331
[34] Corrignan A, Hamard C and Pena O 1999 Superconducting properties of solid solutions $(Mo_6Se_8)Pb_x$ and $Pb_xMo_6Se_8$ in the ternary system Pb-Mo-Se *J. Alloys Compd* **289** 260
[35] Kang Z C, Eyring L, Hinode H, Uchida T, et al. 1994 Structures, structural defects and reactions in a Nickel Chevrel-phase sulphide: A High resolution electron microscopy study *J. Solid State Chem.* **111** 58
[36] Khlybov E P, Kuzmicheva G M and Evdokimova V V 1986 The structure of Mo_2S_3 and of high-pressure modifications of ternary molybdenum sulphides *Russ. J. Inorg. Chemi.* **31** 627
[37] Cors J, Cattani D, Decroux M, Stettler A *et al.* BIDS search
[38] Cattani D, Cors J, Decroux M, Seeber B, et al. 1988 Calorimetric determination of H_{C2} of $PbMo_6S_8$ *Physica* C **153** 461
[39] van der Meulen H P, Perenboom J A A J, Berendschot T T J M, Cors J, et al. 1995 Specific heat of $PbMo_6S_8$ in high magnetic field *Physica B* **211** 269
[40] Bader S D, Knapp G S, Sinha S K, Schweiss P, et al. 1976 Phonon spectra of Chevrel-phase lead and tim molybdenum sulfides: a molecular-crystal model and its implications for superconductivity *Phys. Rev. Lett.* **37** 344
[41] Fradin F Y, Knapp G S, Bader S D, Cinader G, et al. 1976 *Superconductivity in d- and f- Band Metals*, ed D H Douglass p 297
[42] Chen X, Perel A S, Brooks J S, Guertin R P, et al. 1993 Specific heat measurements of pressure-induced reentrant superconductivity in $Eu_{0.9}Ho_{0.1}Mo_6S_8$ *J. Appl. Phys.* **73** 1886
[43] Leigh, N R 2001 The heat capacity of Chevrel phase superconductors exhibiting coexistence of magnetism and supeconductivity Thesis Durham University
[44] Miraglia S, Goldacker W, Flukiger R, Seeber B, et al. 1987 Thermal expansion studies in the range 10 K–1200 K in $PbMo_6S_8$ by means of x-ray diffraction *Mat. Res. Bull.* **22** 795
[45] Alekseevski N E, Nizhankowski V L, Beille J and Lacheisserie E 1988 Investigation of the thermal expansion, electrical resistivity and magnetic susceptibility anisotropy in $PbMo_6S_8$ single crystals *J. Low Temp. Phys.* **72** 241
[46] Seeber B, Glaetzle W, Cattani D, Baillif R, et al. 1987 Thermally induced pre-stress and critical current density of $PbMo_6S_8$ wires *IEEE Trans. Magn.* **23** 1740
[47] Ingle N J C, Willis T C, Larbalestier D C and Meingast C 1998 Effects of hot isostatic pressing on the lattice parameters and the transition temperature of $Pb_{0.8}Sn_{0.2}Mo_6S_8$ *Physica* C **308** 191
[48] Webb A W and Shelton R N 1978 Compressibilities and volume dependence of T_c for eleven Chevrel phase superconductors *J. Phys. F.: Metal Phys.* **8** 261
[49] Goldacker W, Specking W, Weiss F, Rimikis G, et al. 1989 Influence of transverse, compressive and axial tensile stress on the superconductivity of $PbMo_6S_8$ and $SnMo_6S_8$ wires *Cryogenics* **29** 955
[50] Hinks D G, Jorgensen J D and Li H 1984 Oxygen impurity in the chevrel-phase $SnMo_6S_8$ *Solid. State Commun.* **49** 51
[51] Horyn R, Pena O, Wojakowski A and Sergent M 1994 The growth of single crystals of some $REMo_6Se_8$ superconductors *Supercond. Sci. Technol.* **7** 146
[52] Horyn R, Pena O, Geantet C and Sergent M 1989 Kinetics and destruction of Mo-S binary phases and crystal growth of rare-earth molybdenum chalcogenides *Supercond. Sci. Technol.* **2** 71
[53] Krabbes G and Oppermann H 1981 The phase diagram of the Pb-Mo-S system at 1250 K and some properties of the superconducting $PbMo_6S_8$ *Cryst. Res. Technol.* **16** 777

[54] Yamamoto S, Wakihara M and Taniguchi M 1985 Phase relations in the Pb–Mo–S ternary system at 1000°C and the superconductivity of $PbMo_6S_8$ *Mat. Res. Bull.* **20** 1493
[55] Yamasaki H and Kimura Y 1986 The phase field of the chevrel phase $PbMo_6S_8$ at 900°C and some superconducting and structural properties *Mat. Res. Bull.* **21** 125
[56] Holmgren D J, Demers R T, Klein M V and Ginsberg D M 1987 Raman study of phonons in Chevrel-phase crystals *Phys. Rev. B* **36** 1952
[57] Horyn R, le Berre F, Wojakowski A and Pena O 1996 Phase equilibria in the La–Mo–Se system at 1200°C in the vicinity of $LaMo_6Se_6$ and Mo_3Se_4 *Supercond. Sci. Technol.* **9** 1081
[58] Le Berre F, Tshimanga D, Giulloux A, Leclercq J, et al. 1996 Rare-earth doping of the Mo_3Se_4 superconductor *Physica B* **228** 216
[59] Le Berre F, Maho F, Pena O, Horyn R, et al. 1995 Physical and structural properties of Chevrel-phase selenides and $RE_xMo_6Se_8$: crystal growth and mutual solubility *J. Magn. Magn. Mater.* **140** 1171
[60] Decroux M, Selvam P, Cors J, Seeber B, et al. 1993 Overview on the recent progress of Chevrel phases and their impact on the development of $PbMo_6S_8$ wires *IEEE Trans. Appl. Supercond.* **3** 1502
[61] Even-Boudjada S, Burel L, Chevrel R and Sergent M 1998 New synthesis route of $PbMo_6S_8$ superconducting Chevrel phase from ultrafine precursor mixtures: I. PbS, MoS_2 and Mo powders *Mat. Res. Bull.* **33** 237
[62] Selvam P, Cattani D, Cors J, Decroux M, et al. 1992 Superconducting, microstructural and grain boundary properties of hot-pressed $PbMo_6S_8$ *J. Appl. Phys.* **72** 4232
[63] Even-Boudjada S, Tranchant V, Chevrel R, Sergent M, et al. 1999 One of the possible explanations of the major limiting factor at the $PbMo_6S_8$ granular superconductor grain surface *Mater. Lett.* **38** 90
[64] Selvam P, Cattani D, Cors J, Decroux M, et al. 1993 The role of Sn addition on the improvement of J_c in $PbMo_6S_8$ *IEEE Trans. Appl. Supercond.* **3** 1575
[65] Cheggour N, Decroux M, Gupta A, Ritter S, et al. 1993 Superconducting properties of $PbMo_6S_8$ wires with micron grain size obtained from the decomposition of Mo_6S_8 *Proc. ICMAS* **93** 403
[66] Le Berre F, Pena O, Perrin C, Sergent M, et al. 1998 Single crystal studies of the Chevrel phase superconductor $La_xMo_6Se_8$ *J. Solid State Chem.* **136** 151
[67] Pena O, Le berre F, Padiou J, Marchand T, et al. 1998 Single-crystal studies of the Chevrel-phase superconductor $La_xMo_6Se_8$ Q7 *J. Solid State Chem.* **136** 160
[68] Ohtaki R, Zhao B R and Luo H R 1984 Superconducting tunneling on $Cu_xMo_6S_8$ films *J. Low Temp. Phys.* **54** 119
[69] Fumagalli P and Schoenes J 1991 Magneto-optical Kerr-effect study of the high-field superconductors $Eu_{1-x}Pb_xMo_6S_8$ and $Eu_{1-x}Sn_xMo_6S_{8-y}Se_y$ *Phys. Rev.* B **44** 2246
[70] Mattheiss L F and Fong C Y 1977 Cluster model for the electronic structure of the Chevrel-phase comnpound $PbMo_6S_8$ *Phys. Rev.* B **15** 1760
[71] Bullett D W 1977 Relation between Electronic Structure and T_c in Binary and Ternary Molybdenum Chalcogenides *Phys. Rev. Lett.* **39** 664
[72] Prober D E, Schwall R E and Beasley M R 1980 Upper critical fields and reduced dimensionality of the superconducting layered compounds *Phys. Rev.* B **21** 2717
[73] Woolam J A and Somoano R B 1976 Superconducting critical fields of alkali and alkaline-earth intercalates of MoS_2 *Phys. Rev.* B **13** 3843
[74] Mattheis L F 1973 Band structures of transition-metal-dichalcogenide layer compounds *Phys. Rev.* B **8** 3719
[75] Alterovitz S A and Woolam J A 1978 Upper critical field of copper molybdenum sulphide *Solid State Commun.* **25** 141
[76] Cohen R W, Cody G D and Halloran J J 1967 Effect of Fermi-level motion on normal state properties of Beta-tungsten superconductors *Phys. Rev. lett.* **19** 840
[77] Fisk Z and Webb G W 1976 Saturation of the high temperature normal state electrical resistivity of superconductors *Phys. Rev. Lett.* **38** 1084
[78] Meul H W 1986 *Helv. Phys. Acta.* **59** 417
[79] Birrer P, Gygax F N, Hitti B, Lippelt E, et al. 1993 Magnetic penetration depth in the Chevrel-phase superconductors $SnMo_6S_{8-x}$ and $PbMo_6S_{8-x}Se_x$ *Phys. Rev. B* **48** 16589
[80] Schmitt H, Padiou J, Pena O and Sergent M 1991 Crystal growth and single-crystal physical properties of rare-earth-based Chevrel phases $REMo_6S_8$ (RE = Sm, Dy, Tm) *Physica B* **169** 691
[81] Geantet C, Horyn R, Padiou J, Pena O, et al. 1990 Single crystal studies of $REMo_6S_8$ (RE = Er, Lu) *Physica B* **163** 431
[82] Kaiser A B 1997 Comparison of thermopower behaviour in different superconductors *Physica* C **282** 1251
[83] Abrikosov A A 2000 Theory of High-T_c superconducting cuprates based on Experimental evidence *Physica* C **341–348** 97
[84] Furuyama M, Kobayashi N and Muto Y 1989 Electron-phonon interactions in the superconducting Chevrel phase compounds $Mo_6Se_{8-x}S_x$ *Phys. Rev. B* **40** 4344
[85] Pobell F, Rainer D and Wuhl H Electron–Phonon Interaction in Chevrel Phase Compounds, ed O Fischer and M B Maple Q5 p 251
[86] Poppe U and Wuhl H 1981 Tunneling spectrocopy on the superconducting Chevrel-phase compounds $Cu_{1.8}Mo_6S_8$ and $PbMo_6S_8$ *J. Low. Temp. Phys.* **43** 3710

[87] Capone D W, Guertin R P, Foner S and Hinks D G 1984 Effect of pressure and oxygen defects in divalent Chevrel-phase superconductors *Phys. Rev. B* **29** 6375

Q1 [88] Shelton R N 1976 *Second Rochester Conf. on Superconductivity in d- and f-Band Metals* (New York: Plenum)

[89] Shelton R N 1976 *Superconductivity in d- and f- Band Metals* (Plenum).

[90] Lachal B, Bailif R, Junod A and Muller J 1983 Structural instabilities of Chevrel phases: the alkaline earth molybdenum sulphide series *Solid State Commun.* **45** 849

[91] Yao Y S, Guertin R P, Hinks D G, Jorgensen J, et al. 1988 Superconductivity of divalent Chevrel phases at very high pressures *Phys. Rev. B* **37** 5032

[92] Chu C W, Huang S Z, Lin C H, Meng R L, et al. 1981 High-pressure study of the anomalous rare-earth ternaries $Eu_{1.2}Mo_6S_8$ and $Eu_{1.2}Mo_6Se_8$ *Phys. Rev. Lett.* **46** 276

[93] Harrison D W, Lim K C, Thompson J D, Huang C Y, et al. 1981 Observation of the transition from semiconductor to high-T_c superconductor in $(Sn_xEu_{1-x})_yMo_6S_8$ under high pressure *Phys. Rev. Lett.* **46** 280

[94] Harshman D R and Mills A P 1992 Concerning the nature of high T_c superconductivity: Survey of experimental properties and implications for interlayer coupling *Phys. Rev.* B **45** 10684

[95] Batlogg B, Cava R J, Jayaraman A, van Dover R B, et al. 1987 Isostope effect in the High-T_c superconductors $Ba_2YCu_3O_7$ and $Ba_2EuCu_3O_7$ *Phys. Rev. Lett.* **58** 2333

[96] Dallacasa V and Feduzi R 1992 Quantum percolation of high T_c materials: T_c dependence on carrier density *Phys. Lett. A* **170** 153

[97] Morley N A, Leigh N R, Niu H and Hampshire D P 2001 High upper critical field in the Chevrel phase superconductor Lead-molybdenum-sulphide doped with Europium *IEEE Trans. Appl. Supercond.* **11** 3599

[98] Werthamer N R, Helfand E and Hohenberg P C 1966 Temperature and Purity Dependence of the Superconducting Critical Field, H_{C2}. III. Electron Spin and Spin-Orbit Effects *Phys. Rev.* **147** 295

[99] Decroux M, Fischer O, Flukiger R, Seeber S, et al. 1978 Anisotropy of H_{C2} in the chevrel phases *Solid State Commun.* **25** 393

[100] Decroux M and Fischer O 1982 *Critical Fields of Ternary Molybdenum Chalcogenides*, ed O Fischer and M B Maple p 57

[101] Pazol B G, Holmgren D J and Ginsberg D M 1989 Upper critical field anisotropy in the Chevrel phase compound $PbMo_6S_8$ *J. Low. Temp. Phys.* **74** 133

[102] Cave J R 1998 *Handbook of Applied Superconductivity* 1st edn(Bristol: Institute of Physics)

[103] Gorter C J and Casimir H B G 1934 *Physica* **1** 306

[104] Zheng D N, Ramsbottom H D and Hampshire D P 1995 Reversible and irreversible magnetization of the Chevrel phase superconductor $PbMo_6S_8$ *Phys. Rev.* B **52** 12931

[105] Rossel C, Pena O, Schmitt H and Sergent M 1991 On the irreversibility line in the Chevrel phase superconductors *Physica* C **181** 363

[106] Youwen X and Suenaga M 1991 Irreversibility temperature in superconducting oxides: The flux-line-lattice melting, the glass-liquid transition, or the depinning temperatures *Phys. Rev.* B **43** 5516

[107] Yeshurun Y and Malozemoff A P 1988 Giant flux creep and irreversibility in an Y–Ba–Cu–O Crystal: an alternative to the superconducting-glass model *Phys. Rev. Lett.* **60** 2202

[108] Zheng D N and Hampshire D P 1997 The Effect of Gd doping on the critical current of the Chevrel phase superconductor $PbMo_6S_8$ *IEEE Trans. Appl. Supercond.* **7** 1755

[109] Bean C P 1962 Magnetisation of hard superconductors *Phys. Rev. Lett.* **8** 250

[110] Daniel I J and Hampshire D P 2000 Calculations and measurements of the irreversibility field using a vibrating sample magnetometer *Phys. Rev.* B **61** 6982

[111] Ramsbottom H D and Hampshire D P 1999 Flux Penetration measurements and the harmonic magnetic response of hot isostatically pressed $(Pb,Gd)Mo_6S_8$ *J. Appl. Phys.* **85** 3732

[112] Kramer E J 1973 Scaling laws for flux pinning in hard superconductors *J. Appl. Phys.* 44 1360

[113] Ramsbottom H D and Hampshire D P 1997 Improved critical current density and irreversibility line in HIP'ed Chevrel phase superconductor $PbMo_6S_8$ *Physica* C **274** 295

[114] Nakamura T, Hanayama Y, Kiss T, Vysotsky V, et al. 1997 Current–Voltage Characteristics in YBaCuO Thin Films Over More than 13 Decades of Electric-Field *Inst. Phys. Conf. Ser.* **158** p 1017

[115] Gupta A, Decroux M, Willis T C and Fischer O 1994 Resistivity broadening, upper critical fields and irreversibility lines in bulk $PbMo_6S_8$ and $SnMo_6S_8$ Chevrel phase superconductors *Physica* C **235** 2541

[116] Lemee N, Guilloux-Viry M and Sergent M 1998 Superconducting $Cu_2Mo_6S_8$ thin films deposited in-situ by laser ablation on R-plane sapphire *Eur Phys J. Appl. Phys.* **1** 97

[117] Fietz W A and Webb W W 1967 Magnetic properties of some type-II alloy superconductors near the upper critical field *Phys. Rev.* **161** 423

[118] Schauer W and Schelb W 1981 Improvement of Nb_3Sn high field critical current by a two-stage reaction *IEEE. Trans. Magn.* **17** 374

[119] Hampshire D P, Jones H and Mitchell E W J 1984 An in-depth characterisation of $(NbTa)_3Sn$ filamentary superconductor *IEEE. Trans. Magn.* **21** 289

[120] Dew-Hughes D 1974 Flux pinning mechanisms in type II superconductors *Phil. Mag.* **30** 293

[121] Hampshire D P and Jones H 1987 A detailed investigation of the E–J characteristic and the role of defect motion within the flux-line lattice for high-current-density, high field superconducting compounds with particular reference to data on Nb3Sn throughout its entire field-temperature phase space *J. Phys.* C **20** 3533
[122] Gupta A, Decroux M, Sewlvam P, Cattani D, et al. 1994 Critical currents and pinning in powder metallurgicallly processed Chevrel phase bulk superconducting samples *Physica* C **234** 219
[123] Bonney L A, Willis T C and Larbalestier D C 1995 Dependence of critical current density on microstructure in $SnMo_6S_8$ *J. Appl. Phys.* **77** 6377
[124] Karasik V R, Rikel M O, Togonidze T G and Tsebro V I 1985 Investigation of current-carrying capacity of bulk single-phase $PbMo_6S_8$ samples with grains of 0.1 micron size *Sov. Phys. Solid State* **27** 1889
[125] Kramer E J 1975 Microstructure – Critical Current Relationships in Hard Superconductors *J. Electron Mater.* **4** 839
[126] Daniel I J, Zheng D N and Hampshire D P 1997 An Investigation of the Peak Effect in the Chevrel Phase Superconductor Tin Molybdenum Sulphide *IOP Appl. Supercond. Conf.* **2** p 1169
[127] Cattani D, Cors J, Decroux M and Fischer O 1991 Intra- and intergrain critical current in $PbMo_6S_8$ sintered samples *IEEE Trans. Magn.* **27** 950
[128] Herrmann P F, Schellenberg L, Zuccone J, Seeber B, et al. 1992 Investigation of voltage steps of U(I) curves in $PbMo_6S_8$ wires *Physica* C **202** 61
[129] Le Lay L, Willis T C and Larbalestier D C 1991 Magnetization properties of a $SnMo_6S_8$ single crystal *IEEE Trans. Magn.* **27** 954
[130] Hampshire D P 1998 A barrier to increasing the critical current density of bulk untextured polycrystalline superconductors in high fields *Physica* C **296** 153
[131] Rossel C and Fischer O 1984 Critical current Densities in bulk Chevrel phase samples *J. Phys. F: Met Phys.* **14** 455
[132] Rimikis G, Goldacker W, Specking W and Flukiger R 1991 Critical currents in $Pb_{1.2-x}Sn_xMo_6S_8$ wires *IEEE Trans. Magn.* **27** 1116
[133] Selvam P, Cors J, Cattani D and Decroux M et al. 1995 Homogeneity and critical current density of Sn-doped $PbMo_6S_8$ superconductors *Appl. Phys. A* **61** 615
[134] Sergent M, Chevrel R, Padiou J, Pena O, et al. 1984 *Ann. Chim. Fr.* **9** 1069
[135] Willis T C, Jablonski P D and Larbalestier D C 1995 Hot Isostatic Pressing of Chevrel phase bulk and Hydrostatically extruded Wire samples *IEEE Trans. Appl. Supercond.* **5** 1209
[136] Luhman T and Dew-Hughes 1978 Superconducting wires of $PbMo_{5.1}S_6$ by a powder technique *J. Appl. Phys.* **49** 936
[137] Goldacker W, Rimikis G, Specking W, Weiss F, et al. 1989 J_c versus strain investigations of $PbMo_6S_8$ and $SnMo_6S_8$ wires *Adv. Cryo. Eng.*
[138] Yamasaki H, Umeda M, Kosaka S, Kimura Y, et al. 1991 Poor intergrain connectivity of $PbMo_6S_8$ in sintered Mo-sheathed wires and the beneficial effect of hot-isostatic-pressing treatments on the transport critical current density *J. Appl. Phys.* **70** 1606
[139] Kubo Y, Uchikawa F, Utsunomiya S and Noto K et al. 1993 Fabrication and evaluation of small coils using $PbMo_6S_8$ wires *Cryogenics* **33** 883
[140] Kajiyana K, Matsushita T, Yamafuji K, Hamasaki K, et al. 1985 *International symposium on flux pinning and electromagnetic properties in superconductors* (Fukuoka: Matsukuma)
[141] Grant P M 1995 Superconducting superwires *Nature* **375** 107
[142] Ginzburg V L 1957 Ferromagnetic superconductors *Sov. Phys. JETP* **4** 153
[143] Johnston D C and Shelton R N 1977 Magnetic properties of $RE_xMo_6Se_8$ Compounds between 0.7 and 295 K *J. Low Temp. Phys.* **26** 561
[144] Pellizone M, Treyvaud A, Spitzli P and Fischer O 1977 Magnetic susceptibility of $(Rare\ Earth)_xMo_6S_8$ *J. Low Temp. Phys.* **29** 453
[145] Eisaki H, Takagi H, Cava R J and Batlogg B 1994 Competition between magnetism and superconductivity in rare-earth nickel boron carbides *Phys. Rev.* B **50** 647
[146] Majkrzak C F, Shirane G, Thomlinson W, Ishikawa M, et al. 1979 A neutron diffractoion study of the coexistence of antiferromagnetism and superconductivity in $GdMo_6S_8$ *Solid State Commun* **31** 773
[147] Thomlinson W, Shirane G, Moncton D E, Ishikawa M, et al. 1981 Magnetic order in superconducting $TbMo_6S_8$, $DyMo_6S_8$ and $ErMo_6S_8$ *Phys. Rev.* B **23** 4455
[148] Morales F, Escudero R, Briggs A, Monceau P, et al. 1996 Point contact spectroscopy on the ferromagnetic superconductor $HoMo_6S_8$ *Physica* B **218** 193
[149] Hampshire D P 2001 The non-hexagonal flux-line lattice in superconductors *J. Phys* C **13** 6095
[150] Jaccarino V and Peter M 1962 Ultra-high-field superconductivity *Phys. Rev. Lett.* **9** 290
[151] Blount E I and Varma C M 1979 Electromagnetic effects near the Superconductor-to-Ferromagnet Transition *Phys. Rev. Lett.* **42** 1079
[152] Watanabe K, Awaji S, Motokawa M, Mikami Y, et al. 1998 15 T Cryocooled Nb_3Sn superconducting magnet with a 52 mm room temperature bore *Japan. J. Appl. Phys.* **37** L1148

Further Reading

Maple M B and Fischer Ø 1982 *Superconductivity in Ternary Compounds Vol. I and II – Structural, Electronic and Lattice Properties* Berlin: Springer

These two volume texts were written by many of the individual researchers involved in the intensive research of the seventies. The texts include an excellent compendium of many of the material properties for Chevrel phase superconductors — to avoid extending our reference list considerably we have quoted these texts as a source rather than citing the several hundred papers quoted therein.

Evetts J 1992 *Concise Encyclopaedia of Magnetic and Superconducting Materials* Oxford, UK: Pergamon

Series of compact, introductory articles predominantly on the science and technology of magnetic and superconducting materials.

Pena O Sergent M 1989 Rare earth based Chevrel phases $REMo_6X_8$: crystal growth, physical and superconducting properties *Prog. Solid State Chem.* **19** 165–281

A very interesting comprehensive review of single crystal growth and properties. Great detail is provided on the chemistry and materials science of rare earth materials.

Fischer Ø 1978 Chevrel phases: superconducting and normal state properties *Appl. Phys.* **16** 1–28

Excellent older review of the properties of Chevrel phase superconductors.